

Tocotrienols improve urban particulate matter-induced skin damages by regulating skin barrier function and ROS/MAPK signalling pathway in keratinocytes

Juvenia Rui En Neo^{a,1}, Zi Ning Teo^{b,1}, Jolene Shi En Yeo^b, Cassey Kai Sing Ng^b, Cheryl Wei Ling Teo^a, Yee Wei Ung^c, Wei Ney Yap^{a,*}

^a Research and Development Department, Davos Life Science Pte Ltd, 3, Biopolis Drive, #04-19, Synapse, 138623, Singapore

^b School of Biological Sciences, Nanyang Technological University, 50 Nanyang Avenue, 639798, Singapore

^c Research and Development Department, KL-Kepong Oleomas (KLK Oleo), Level 8, Menara KLK, No 1 Jalan PJU 7/6, Mutiara Damansara, 47810, Petaling Jaya, Selangor, Malaysia

ARTICLE INFO

Keywords:

Particulate matter
Tocotrienol-rich fraction
Antioxidant
Anti-inflammatory
Skin barrier

ABSTRACT

Urban particulate matter (PM) is a major air pollutant that triggers molecular processes and is detrimental to the skin. We investigated the protective effects of tocotrienol-rich fraction (TRF) against urban PM-induced skin ageing, inflammation, and skin barrier dysfunction in human epidermal keratinocytes. Alpha-tocopherol (α TP) and retinoic acid (RA) were used as comparators. Our results showed that TRF significantly restored cell viability and alleviated increased intracellular reactive oxygen radicals in PM-treated keratinocytes. In addition, TRF significantly downregulated the activation of mitogen-activated protein kinases in PM-stimulated keratinocytes. This was substantiated by lower protein expression in the phosphorylation of extracellular signal-regulated kinase, Jun N-terminal kinase, and p38. This resulted in the inhibition of cyclooxygenase-2 expression, which is a downstream inflammatory mediator. TRF significantly protected skin barrier function upon exposure to PM by upregulating filaggrin, transglutaminase-1, and involucrin. In contrast, α TP and RA did not exhibit protective effects against skin damages in the PM-treated keratinocytes. Overall, this study suggests that TRF possesses antioxidant, anti-inflammatory, and skin barrier protective properties, and may serve as a potential ingredient in personal care and cosmeceutical industries to combat skin damage due to air pollution.

1. Introduction

Air pollution is the world's largest environmental health risk owing to rapid urbanisation and industrialisation. The World Health Organization (WHO) estimates that the inhalations of air pollutants (outdoors and in households) causes millions of premature deaths annually owing to respiratory infection, chronic obstructive pulmonary disease, heart disease, and lung cancer (Organization, W. H., 2021). Particulate matter (PM) is a complex mixture of particles and droplets suspended in the air and comprises inorganic and organic compounds, such as polyaromatic hydrocarbons, trace elements, water-soluble ions, soil, and dust (Yang et al., 2021). Owing to their microscopic size, PM is easily inhaled and

can even enter the bloodstream (Agency U.S.E.P., 2020). Notably, PM can carry additional toxic substances, such as bacteria and carcinogens, on its surface and exert harmful effects on human health. PM has been classified into three categories based on particle size: PM0.1 (particles $\leq 0.1 \mu\text{m}$ in diameter), PM2.5 (particles $\leq 2.5 \mu\text{m}$ in diameter), and PM10 (particles $\leq 10 \mu\text{m}$ in diameter), which are called ultrafine, fine, and coarse particles, respectively. Numerous studies have revealed that PM2.5 has long-term effects on cardiovascular and respiratory systems, and repeated PM2.5 skin exposure aggravates cutaneous diseases (Kloog et al., 2013; Ngoc et al., 2017; Loxham et al., 2019; Kim et al., 2021).

The skin acts as the primary biological shield against PM and is most exposed to environmental contaminants and stressors (Byrd et al., 2018;

Peer review under responsibility of Turkish National Committee for Air Pollution Research and Control.

* Corresponding author.

E-mail addresses: ruien.neo@davoslife.com (J.R.E. Neo), ZTEO016@e.ntu.edu.sg (Z.N. Teo), JYEO040@e.ntu.edu.sg (J.S.E. Yeo), NGKA0018@e.ntu.edu.sg (C.K.S. Ng), weiling.teo@davoslife.com (C.W.L. Teo), yw.ung@klkoleo.com (Y.W. Ung), weiney.yap@davoslife.com (W.N. Yap).

¹ Both authors contributed equally to this study.

<https://doi.org/10.1016/j.apr.2022.101564>

Received 25 March 2022; Received in revised form 8 September 2022; Accepted 9 September 2022

Available online 13 September 2022

1309-1042/© 2022 Turkish National Committee for Air Pollution Research and Control. Production and hosting by Elsevier B.V. This is an open access article under the CC BY-NC-ND license (<http://creativecommons.org/licenses/by-nc-nd/4.0/>).

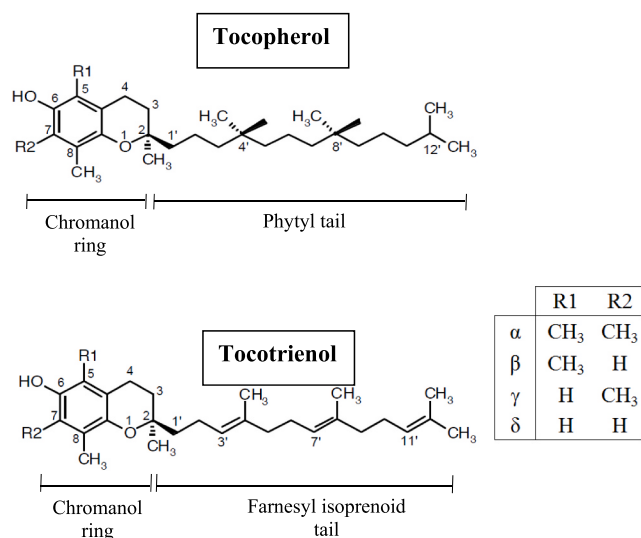


Fig. 1. Structure and natural form of vitamin E family – tocopherol and tocotrienol.

Nguyen and Soulika 2019). Prolonged exposure to PM, which exceeds the normal defensive potential of the skin, may have profound adverse effects. PM can penetrate the human skin surface either through hair follicles or across the stratum corneum (Kim et al., 2016). Consequently, the skin barrier mechanism is compromised, leading to deep penetration of PM into the dermal layer of the skin. This causes skin damage, resulting in the aggravation of skin disorders, such as atopic dermatitis and eczema, all of which involve an impaired skin barrier (Ngoc et al., 2017; Dijkhoff et al., 2020). PM has also been found to activate matrix metalloproteinases (MMPs), resulting in accelerated skin ageing and loss of skin elasticity (Fu et al., 2021). PM exerts its toxicity on the skin through four main mechanisms: generating free radicals, activating the aryl hydrocarbon receptor (AhR), inducing the inflammatory cascade, and disrupting the skin barrier (Dijkhoff et al., 2020).

To date, many protective measures against PM-induced skin damage have influenced the ability of natural ingredients, including antioxidants, to reduce oxidative stress and pro-inflammatory responses. Vitamin E is a ubiquitous antioxidant naturally found in food sources, such as plant-based oils, nuts, and seeds (Mohd Zaffarin, Ng et al., 2020). It is known for its various antioxidative activities and is closely linked to maintaining skin health. Studies have reported that a loss of serum vitamin E results in inflammatory skin diseases, such as acne and atopic dermatitis (Liu et al., 2021). Vitamin E occurs in eight different fat-soluble forms: α -, β -, γ -, and δ -tocopherol (TP) and α -, β -, γ -, and δ -tocotrienol (T3). The structural difference between TPs and T3s is the fully saturated hydrocarbon tail TPs, whereas T3s contain three unsaturated double bonds in their hydrocarbon tails (Fig. 1). This unsaturated side chain allows more efficient tissue penetration, which explains its superior anti-inflammatory and antioxidant properties. T3s are also more evenly distributed in the fatty layers of the cell membrane, enabling them to protect cells against lipid peroxidation, particularly in areas of the body with a high lipid content, such as the skin (Niki 2015; Peh et al., 2016). Furthermore, T3s reportedly exhibit anti-inflammatory effects by suppressing nuclear factor-kappa B (NF- κ B), tumor necrosis factor-alpha (TNF- α), and cyclooxygenase 2 (COX-2) (Mohd Zaffarin, Ng et al., 2020; Wong et al., 2020). The ability to suppress the expression of these cytokines greatly reduces inflammation in the body.

Although a few studies have elucidated the benefits of T3s in the skin, there are no studies on the underlying mechanism of T3s on PM exposure. Thus, this study conducted several experiments to understand how T3s act as an antioxidant and anti-inflammatory ingredient to protect the skin after prolonged PM exposure. Our experiment used,

tocotrienol-rich fraction (TRF), a commercially available T3 mixture. This TRF comprised four T3 isoforms and one TP isoform, α -tocopherol (α TP). Two comparators were used in the study, namely α TP and retinoic acid (RA). α TP is common form of vitamin E owing to its high bioavailability and abundance in the human body (Peh et al., 2016). RA is commonly used in immune-mediated skin diseases, such as acne and psoriasis, as it reduces MMP and inflammatory cytokines production, enhances type I collagen, and transforms growth factor beta production (Oliveira et al., 2018). However, long-term use of RA can contribute to a tolerance that eventually disrupts the epidermal barrier (Szymanski et al., 2020). To the best of our knowledge, this is the first study to demonstrate the efficacy of TRF against urban PM-induced skin damage in comparison with α TP and RA, the two other common skin care ingredients in the market.

2. Materials and methods

2.1. Cell culture and reagents

Associate Professor Dr. Gautam Sethi (National University of Singapore, Singapore) supplied the human epidermal keratinocyte cell line (HaCaT). The cells were grown in high glucose Dulbecco's modified Eagle's medium (DMEM) from Nacalai Tesque (Kyoto, Japan) supplemented with 10% foetal bovine serum (FBS) from GE Healthcare (Pasching, Austria) and 1% penicillin-streptomycin from Gibco (Utah, USA). The cells were maintained in 5% CO₂ at 37 °C. PM (SRM 1649b) was obtained from the National Institute of Standards and Technology (Gaithersburg, MD, USA). Monoclonal antibodies against phospho-p38, total p38, phospho-c-Jun N-terminal kinase 1/2 (JNK 1/2), total JNK 1/2, phospho-extracellular signal-regulated kinase 1/2 (ERK1/2), total ERK 1/2, cleaved caspase-3, and mitogen-activated protein kinase (MAPK) inhibitors SB203580, SP600125, and U0126 were obtained from Cell Signalling (Danvers, MA, USA). The monoclonal antibodies against COX-2 and β -actin were purchased from Research Instruments (Singapore) and Santa Cruz Biotechnology (Santa Cruz, CA, USA), respectively. Enzyme-linked immunosorbent assay (ELISA) kits for filaggrin (FLG), transglutaminase-1 (TGM-1), and involucrin (IVL) were purchased from Biorbyt (Cambridge, United Kingdom), BlueGene Biotech (Shanghai, China), and FineTest Biotech (Wuhan, China), respectively. Phosphate-buffered saline (PBS) and methanol were purchased from Gibco (Utah, USA) and Tedia (Ohio, USA), respectively. Moreover, 2',7'-dichlorofluorescein diacetate (DCFH-DA), 3-(4,5-Dimethyl-2-thiazolyl)-2,5-diphenyl-2H-tetrazolium bromide (MTT), 2,2-diphenyl-1-picrylhydrazyl-hydrate (DPPH), trolox, crystal violet, α TP, and RA were obtained from Sigma-Aldrich (St. Louis, MO, USA). TRF with 95% purity (DavosLife E3) was supplied by Davos Life Science Sdn Bhd (Malaysia).

2.2. Antioxidant assay

The DPPH free radical assay was performed according to the method of Brand-Williams et al. with some modifications (Brand-Williams et al., 1995). Serial dilutions of TRF, α TP, RA, and trolox (10 μ M, 25 μ M, 50 μ M, 100 μ M, 250 μ M, 500 μ M, and 1000 μ M) were prepared in ethanol. Each test sample solution (10 μ L) was added to a 96-well plate in triplicate, followed by 190 μ L of 0.12 mM DPPH solution. The mixture was incubated for 30 min with gentle shaking. The decrease in absorbance was measured at 517 nm using an EnSpire® Multimode Plate Reader (PerkinElmer, Waltham, MA, USA).

2.3. p.m. preparation

The PM-induced model adopted the method described in a previous study (Lee et al., 2016). We used PM2.5, which is a standard urban dust (SRM 1649B) primarily comprising polycyclic aromatic hydrocarbons (PAHs), nitro-substituted PAHs (nitro-PAHs), polychlorinated biphenyl

(PCB) congeners, chlorinated pesticides, and inorganic constituents in atmospheric particulate material. Briefly, an SRM 1649B urban dust suspension was prepared in cell culture media at a concentration of 1000 µg/mL. The suspended particles were vortexed and sonicated for 30 min before use to avoid the agglomeration of the suspended PM_{2.5}. Experiments were performed with the stock solution within 1 h of PM preparation to circumvent variations in PM composition in the solution. The cells were exposed to a PM concentration of 100 µg/mL for 24 h.

2.4. Colony forming assay

HaCaT cells were plated onto 10 cm dishes and pre-treated with 20 µM TRF, 20 µM αTP, and 1 µM RA for 24 h. PM (100 µg/mL) was added to the cells for 24 h, followed by the same individual treatment dosage for another 24 h. The cells were then harvested, plated at 200 cells per well in 24-well plates, and incubated at 37 °C for one week. The colonies were then fixed with 100% methanol for 20 min and stained with 0.5% crystal violet for 5 min. The cells were rinsed with PBS, inverted onto the tissue, and dried overnight. The cells were then observed under a Nikon TE2000-U inverted microscope (Nikon, Tokyo, Japan), and the colonies were counted.

2.5. Cell proliferation assay

Cell viability was examined using an MTT assay. HaCaT cells were seeded in 96-well plates and pre-treated for 24 h with 20 µM TRF, 20 µM αTP, and 1 µM RA. The cells were then incubated with 100 µg/mL PM for 24 h. Following PM supplementation, HaCaT cells were incubated with the same treatment dosage for another 24 h. MTT (5 mg/mL) was then added to each cell-containing well and incubated for 2 h. The cell culture medium was replaced with dimethyl sulfoxide (DMSO) to solubilise purple formazan. The absorbance was read at 595 nm and 750 nm using an EnSpire® Multimode Plate Reader (PerkinElmer, Waltham, MA, USA).

2.6. Intracellular reactive oxygen species (ROS) assay

HaCaT cells were seeded into 96-well plates and incubated overnight. The next day, the cells were treated with 20 µM TRF, 20 µM αTP, and 1 µM RA for 24 h. The cells were then treated with 100 µg/mL PM for 24 h. Afterward, the medium was removed, and the cells were washed with KRH buffer and incubated with 100 µM DCFH-DA in the loading medium in 5% CO₂ at 37 °C for 30 min. After the DCFH-DA was removed, the cells were washed, and the fluorescence from each well was measured using an EnSpire® Multimode Plate Reader (PerkinElmer, Waltham, MA, USA). The excitation and emission filters were set to 485 nm and 530 nm, respectively. The percentage increase in DCFH fluorescence per well was calculated using the following equation:

$$\frac{(F_{t_{30\text{min}}} - F_{t_{0\text{min}}})}{F_{t_{0\text{min}}}}$$

$F_{t_{30\text{min}}}$ = fluorescence at 30 min

$F_{t_{0\text{min}}}$ = fluorescence at 0 min

The values of the respective treatment groups were normalized to sham to obtain the fold change and show the differences in ROS expression.

2.7. ELISA

HaCaT cells were pre-treated with 20 µM TRF, 20 µM αTP, or 1 µM RA for 24 h, followed by exposure to 100 µg/mL PM for another 24 h. Cell pellets were collected and stored at -80 °C until further analysis. FLG, TGM-1, and IVL were quantified by ELISA according to the manufacturer's instructions.

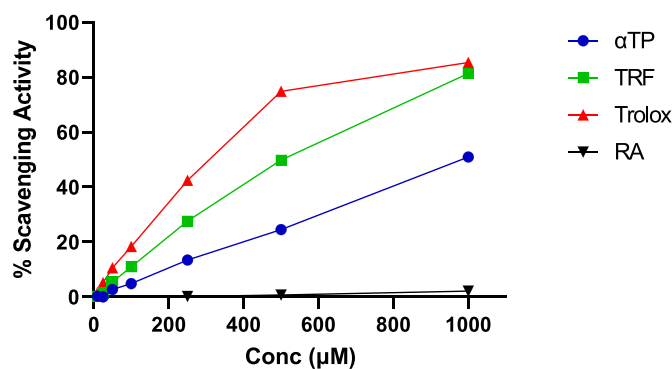


Fig. 2. Antioxidant activity of TRF, αTP, RA, and trolox using DPPH assay. Serial dilution of each treatment (10 µL) (10 µM, 25 µM, 50 µM, 100 µM, 250 µM, 500 µM and 1000 µM) were added to a 96-well culture plate, following 190 µL of 0.12 mM DPPH solution. The mixture was incubated for 30 min with gentle shaking. The percentage scavenging activity was calculated in the trend graph.

2.8. Western blotting

Whole-cell lysates were collected by suspending cell pellets in radioimmunoprecipitation assay (RIPA) lysis buffer containing 50 mM Tris-HCl pH 8.0, 150 mM sodium chloride (NaCl), 1 mM ethylenediaminetetraacetic acid (EDTA), 1% v/v Nonidet P-40 (NP-40), 0.5% v/v sodium deoxycholate, and 0.1% v/v sodium dodecyl sulfate (SDS), supplemented with protease and phosphatase cocktail inhibitors (Roche, Basel, Switzerland). The protein concentration was measured using a DC Protein Assay kit (Bio-Rad, Hercules, CA, USA) in a 96-well plate. Reagents A (25 µL) and B (200 µL) were added to 5 µL of the cell lysate. After 15 min of incubation, the absorbance at 750 nm was measured using the EnSpire® Multimode Plate Reader (PerkinElmer, Waltham, MA, USA). Protein standards were prepared using bovine serum albumin (Sigma-Aldrich, St. Louis, MO, USA). Protein samples underwent SDS polyacrylamide gel electrophoresis (SDS-PAGE) at 20 mA for 1 h using the Bio-Rad Mini-PROTEAN 3 Cell system (Hercules, CA). They were transferred onto a polyvinylidene difluoride (PVDF) membrane (Amersham, Piscataway, NJ, USA) via the wet transfer method at 100 V for 90 min using the Bio-Rad Mini Trans-Blot Electrophoretic Transfer Cell system (Hercules, CA). The membrane was then blocked with 10% (w/v) non-fat milk (Bio-Rad Laboratories, Inc. Hercules, CA) in Tris-buffered saline (TBS) with 0.1% v/v Tween-20 (TBS-T). The blots were washed three times with TBS-T and incubated with their respective antibodies at 4 °C overnight. The blots were then washed with TBS-T to remove the unbound primary antibodies before being exposed to IgG-HRP-conjugated secondary antibodies in 5% w/v non-fat milk in TBS-T for 1 h at room temperature. Unbound secondary antibodies were removed by washing the blots with TBS-T. Chemiluminescent signals were visualised using an ECL western blotting system (Amersham, Piscataway, NJ, USA). Image Lab™ software (Bio-Rad, Hercules, CA, USA) was used for densitometric analysis.

2.9. Statistical analysis

All data are presented as the mean ± standard error. Significant differences in all the data were analysed using GraphPad Prism version 9.1.0 (GraphPad Software, San Diego, CA) with a one-way analysis of variance (ANOVA), followed by Tukey's post hoc test. $P < 0.05$ (*) was considered statistically significant.

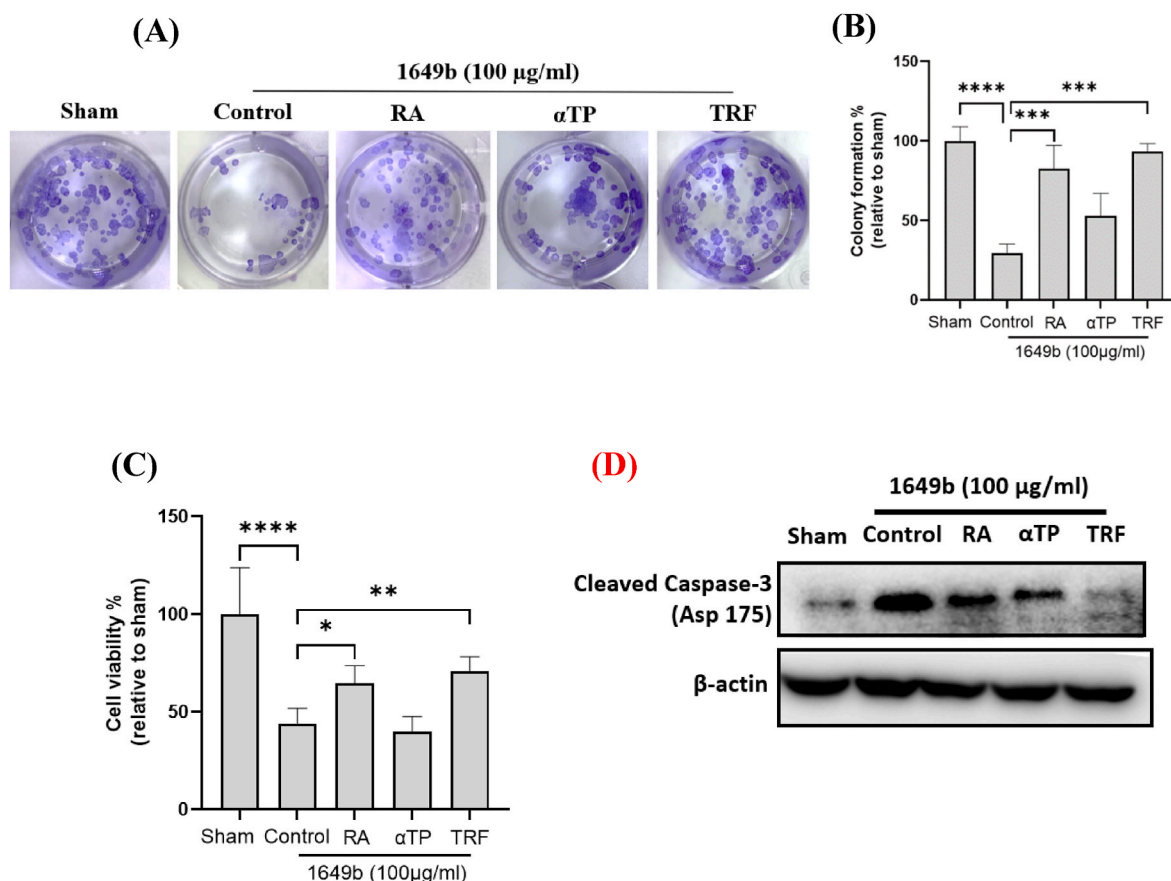


Fig. 3. Effect of TRF, αTP, and RA treatments on colony forming assay, cell proliferation, and apoptosis assay after PM_{2.5} induction. (A) HaCaT cells were pre-treated with RA (1 µM), αTP (20 µM) or TRF (20 µM) for 24 h followed by 100 µg/ml PM_{2.5} exposure. The cells continue with post-treatment with the individual treatments for 24 h. 200 cells/ml were then seeded on 24-well culture plate. A total of 7 days later, cells were stained with 0.5% crystal violet after the colony has formed. (B) The colony formation percentage was calculated from numbers of colony formed and normalized from the sham (without PM_{2.5} exposure). (C) The cell proliferation was determined by MTT assay after the cells were pre- and post-treated with respective treatments for 24 h before the PM_{2.5} exposure. (D) Activation of apoptotic marker (cleaved caspase 3) by PM_{2.5} exposure was determined western blotting. Data are expressed as mean ± standard deviation of three independent experiments. **P* < 0.05, ***P* < 0.01, ****P* < 0.001 and *****P* < 0.0001, as assessed by one-way ANOVA, followed by Tukey's post hoc test. TRF, tocotrienol-rich fraction; αTP, alpha tocopherol; RA, retinoic acid; MTT, 3-(4,5-dimethylthiazol-2-yl)-2,5-diphenyl tetrazolium bromide; 1649b, PM_{2.5} (particulate matter that has the diameter of less than 2.5 µm).

3. Results and discussion

3.1. TRF showed higher antioxidant activity in DPPH assay

Antioxidants, such as TRF, αTP, and RA, process and remove the harmful effects of ROS, which are highly reactive chemical molecules produced to degrade damaged tissue structures and extract invading microorganisms. Typically, this occurs through free radical scavenging, which allows antioxidants to indirectly improve antioxidant defences of the body (Dijkhoff et al., 2020; Gulcin 2020). DPPH is a violet radical molecule, and the assay measures antioxidant activity based on the molecule reducing to a pale-yellow colour. In this case, the DPPH assay can provide details on the reducing capacity of the antioxidant and its ability to donate hydrogen atoms (Sirivibulkovit et al., 2018).

In this study, we examined the ability of four antioxidants: αTP, TRF, RA, and trolox (positive control). As Fig. 2 shows, αTP, TRF, and Trolox had varying scavenging effects, whereas RA provided a near-zero effect. Based on these results, αTP and TRF exhibited scavenging activity in a dose-dependent manner, showing 50% and 80% effects, respectively, at a concentration of 1000 µM. Notably, the activity of 1000 µM TRF was comparable to that of Trolox, a standard antioxidant.

Vitamin E (T3s and TP) are best known for their antioxidant and anti-inflammatory activities (Ungurianu et al., 2021). Although T3 and αTP have similar properties, their mechanisms of action differ. αTP

antioxidant functions in the form of a radical-chain breaker, which protects cellular membranes from lipid peroxyl radicals. However, αTP does not physiologically act as an antioxidant. Alternatively, it functions as a cell signalling molecule capable of regulating gene expression or signalling cascades (Azzi 2007). Conversely, T3s function as unique antioxidants, as they can scavenge reactive nitrogen species in addition to usual ROS. T3s can also inhibit the upregulation of several inflammatory molecules and increase antioxidant modulatory enzymes through selective control of the Kelch-like ECH-associated protein 1-nuclear factor (erythroid-derived 2)-like 2 (Keap1-NRF2) pathways, which are downstream of MAPK. T3s also exhibit considerably stronger anti-inflammatory effects as they can inhibit NF-κB and signal transducer and activator of transcription 3 (STAT3), which are two important inflammatory transcription factors (Ahsan et al., 2014; Aggarwal et al., 2019). RA, a vitamin A metabolite, is crucial in regulating and maintaining immune responses (Oliveira et al., 2018). RA receptors (RARs) and retinoid X receptors (RXRs) mediate the effects of RA. Upon binding to the RAR/RXR heterodimer, RXR ligands affect several signalling pathways (Marill et al., 2003).

T3s, in this case, serve as a more advantageous antioxidant, as they can alleviate inflammation by directly acting on inflammatory pathways, compared to αTP or RA, which modulate the pathways independently.

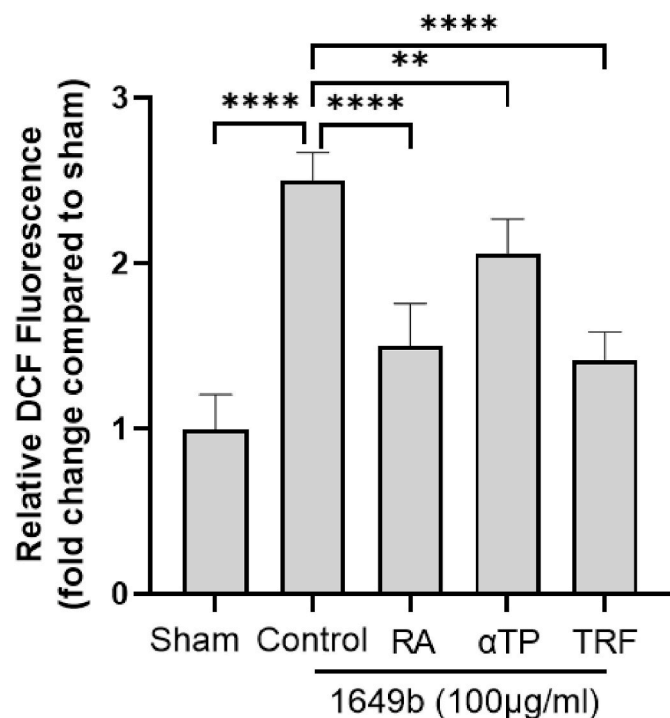


Fig. 4. Effects of TRF, α TP, and RA treatments on the generation of ROS upon PM_{2.5} induction. HaCaT cells were pre-treated with TRF (20 μ M), α TP (20 μ M) or RA (1 μ M) followed by 100 μ g/ml PM exposure. After 30 min post-induction, the intracellular ROS levels were determined using the fluorogenic probe DCFH-DA. The relative intensity of DCF fluorescence is shown in the bar graph. Data are expressed as mean \pm standard deviation of three independent experiments. ** $P < 0.01$ and **** $P < 0.0001$, as assessed by one-way ANOVA, followed by Tukey's post hoc test. TRF, tocotrienol-rich fraction; α TP, alpha tocopherol; RA, retinoic acid; ROS, reactive oxygen species; DCF, dichlorofluorescein; DCFH-DA 2',7'-dichlorofluorescein diacetate; 1649b, PM_{2.5} (particulate matter that has the diameter of less than 2.5 μ m).

3.2. TRF reduced PM_{2.5}-induced cytotoxicity and oxidative damages in HaCaT cells

One of the main mechanisms through which PM exerts toxicity on the skin involves inducing excessive ROS production. PM, such as diesel, PAHs, and transition metals, triggers ROS generation through oxygen reduction, redox activity, and Fenton reactions, respectively. Additionally, these compounds can increase ROS generation by inducing mitochondrial stress and stimulating ROS-producing enzymes (Dijkhoff et al., 2020). Furthermore, PM can bind to AhR, a cytosolic ligand-activated transcription factor activated by environmental pollutants. Upon activation, AhR translocates to the nucleus forming a dimer with the AhR nuclear translocator. This complex then binds to the promoter regions that contain xenobiotic response elements, promoting the transcription of phase I metabolism, phase II metabolism, and AhR repressor genes. These enzymes metabolise PAHs, producing metabolites that can induce cell damage by forming DNA and protein adducts. Notably, this also results in further ROS formation (Dijkhoff et al., 2020). Under normal physiological conditions, cells can remove ROS produced via their cellular antioxidative and scavenging systems through superoxide dismutases or glutathione (Marengo et al., 2016). However, when ROS production exceeds the antioxidant defence system, oxidative stress occurs and aggravates pathological processes, such as tissue damage, DNA damage, protein carbonylation, and lipid peroxidation (Lee et al., 2016; Dijkhoff et al., 2020). Increased PM-induced ROS production can inhibit the intracellular antioxidative system, ultimately reducing keratinocyte viability (Piao et al., 2018).

In this study, PM_{2.5}-induced cell viability and oxidative damage in

HaCaT cells were evaluated by colony formation, a cell proliferation assay, an apoptotic marker, and intracellular ROS levels. Fig. 3(A) and (B) show that 100 μ g/mL PM_{2.5} significantly suppressed colony formation in HaCaT cells after 24 h of exposure. Among the treatments, 20 μ M TRF and 1 μ M RA but not 20 μ M α TP restored the number of colonies after PM_{2.5} exposure. These results were validated using a cell proliferation assay. PM_{2.5}-induced keratinocytes showed less than 50% of the cell survival relative to sham. However, the TRF and RA treatments significantly restored the cellular proliferation rate. In contrast, α TP had a less prominent effect (Fig. 3(C)). Consistent with the MTT assay, procaspase 3 activation, as evidenced by cleaved caspase 3, was observed in HaCaT cells exposed to PM_{2.5}. As Fig. 3(D) shows, TRF treatment significantly reduced PM_{2.5}-induced apoptosis in comparison with α TP and RA.

One of the speculated mechanisms of decreased cellular proliferation is correlated with increased intracellular ROS generation upon PM exposure (Piao et al., 2018). As Fig. 4 shows, upon exposure to PM_{2.5}, the intracellular ROS level was stimulated approximately 2.5-fold compared to that in the sham group. At the same concentration (20 μ M), TRF was more effective than α TP at reducing intracellular ROS concentration after exposure to 100 μ g/mL PM_{2.5}. Conversely, when 1 μ M RA was used, we observed a ROS scavenging effect similar to that of 20 μ M TRF. Overall, these results indicate that TRF inhibits PM_{2.5}-induced cytotoxicity by suppressing excessive ROS production.

3.3. TRF suppressed PM_{2.5}-induced MAPK and COX-2 activation in HaCaT cells

MAPK is a pathway that helps relay, amplify, and integrate signals from stimuli and elicit responses, such as cellular proliferation, inflammatory responses, and apoptosis (Zhang and Liu 2002). Typically, during the onset of skin inflammation, the proteins involved in the MAPK pathway are phosphorylated and activated. This triggers the downstream NF- κ B pathway, increasing inducible nitric oxide synthase and COX-2 expression, which are inflammation mediators (Liu et al., 2018). In cells exposed to PM, MAPK members p38, JNK, and ERK can be phosphorylated (Huang et al., 2018; Zhen et al., 2019). This is possibly due to the action of AhR, which engages in crosstalk with the MAPK pathway. This causes proto-oncogene tyrosine-protein kinase (c-Src) activation, which in turn binds to the epidermal growth factor receptor (EGFR) and activates the pathway (Dijkhoff et al., 2020; Shi et al., 2021). In HaCaT cells, ERK is activated, leading to subsequent p38 and NF- κ B activation (Lee et al., 2016). NF- κ B is a transcription factor comprising five inducible transcription factors that induce pro-inflammatory genes, including chemokines and cytokines. We observed increased COX-2 and prostaglandin E2 (PGE2) expression and eventually ROS generation in PM-induced cells. Furthermore, upon PM-induced activation, JNK induces the phosphorylation of activator protein (AP-1) transcription complexes c-Jun and c-Fos (Lee et al., 2016). AP-1 activation then results in an increase in MMP expression, which mediates the decomposition of extracellular matrix elements, such as collagen and elastic fibres, leading to skin barrier impairment (Rinnerthaler et al., 2015).

Considering that the MAPK signalling pathway is involved in PM-mediated inflammation, apoptosis, and skin barrier function modulation, we investigated MAPK-related proteins via western blotting. Fig. 5 (A)–(C) show that 100 μ g/mL PM_{2.5} activated p38, JNK1/2, and ERK phosphorylation in HaCaT cells compared to the levels in control cells. However, the phosphorylation of these proteins was significantly downregulated by the 20 μ M TRF treatment. Nevertheless, the 1 μ M RA or 20 μ M α TP treatments did not strongly inhibit MAPK phosphorylation. We investigated COX-2 expression levels to examine the downstream effects of MAPK activation. PM_{2.5}-induction increased the expression of COX-2 proteins, whereas TRF greatly inhibited its expression (Fig. 5(D)). Reduced COX-2 expression in TRF-treated HaCaT cells corroborates a study on TRF-treated PM-induced THP-1

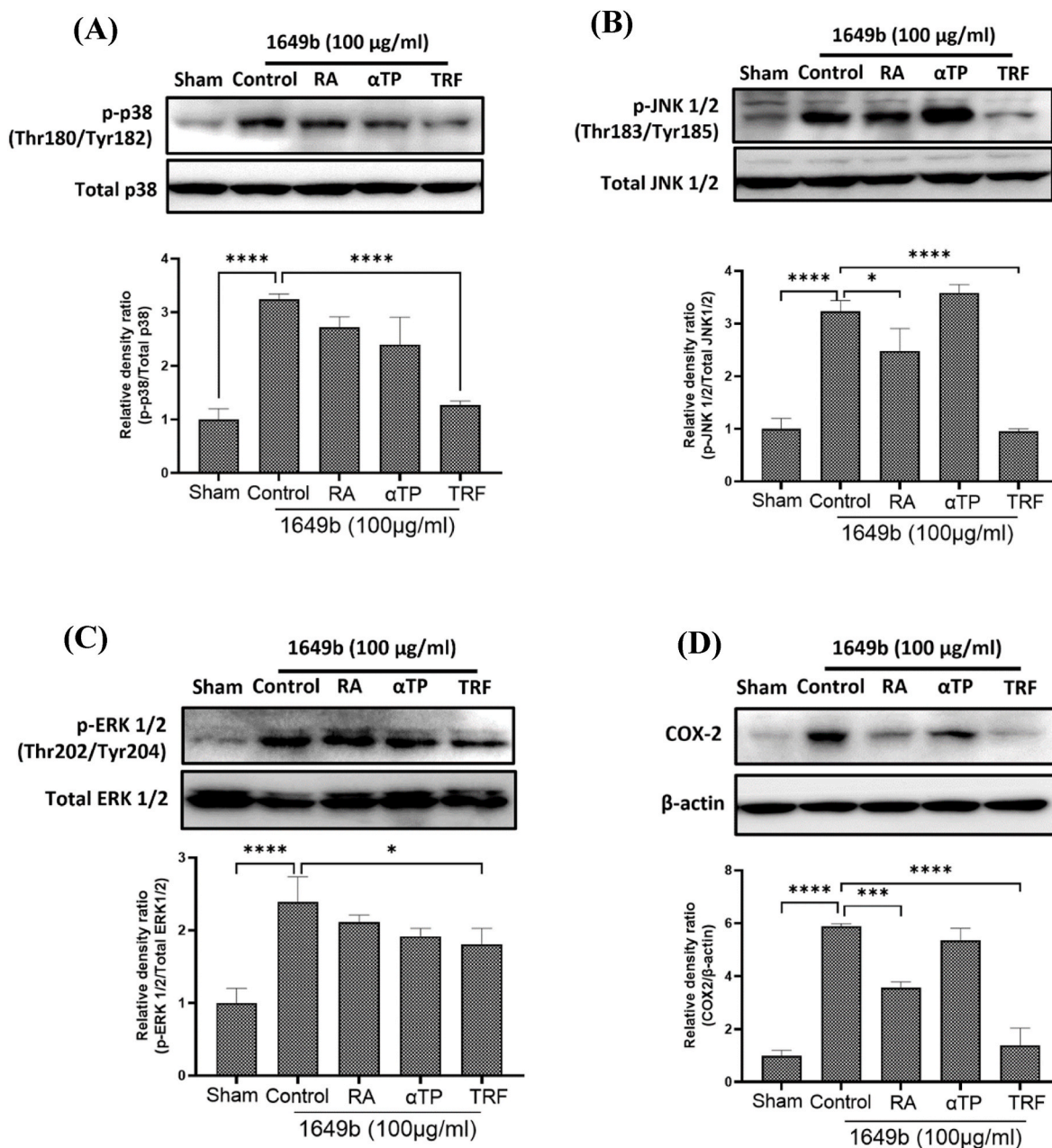


Fig. 5. Mechanism of action of TRF, αTP and RA treatments in PM_{2.5}-induced MAPKs cell signalling cascades. (A to C) TRF treatment significantly inhibited p38, JNK 1/2, and ERK 1/2 phosphorylation after 100 μg/ml PM_{2.5} exposure, but not αTP and RA. (D) Suppression of COX-2 expression by TRF in stimulated PM. Note that sham exposure did not induce the activation of the pathways. Blots are representative of three independent experiments. The relative protein expression levels were quantified by densitometric analysis. Data are expressed as mean ± standard deviation of three independent experiments. **P* < 0.05, ****P* < 0.001 and *****P* < 0.0001, as assessed by one-way ANOVA, followed by Tukey's post hoc test. RA, TRF, tocotrienol-rich fraction; αTP, alpha tocopherol; RA, retinoic acid; MAPKs, mitogen-activated protein kinases; JNK, c-jun N-terminal kinase; ERK, extracellular signal-regulated kinase; COX-2, cyclooxygenase-2; 1649b, PM_{2.5} (particulate matter that has the diameter of less than 2.5 μm).

promonocytic cells (Wu et al., 2008). To a lesser extent, αTP and RA could suppress COX-2 expression. We anticipated that COX-2 inhibition by TRF would downregulate the downstream molecule PGE₂. A study that showed that the attenuation of PGE₂ production by T3s is more efficient than TPs in interleukin (IL)-1 beta-stimulated A549 cells supports these findings (Jiang et al., 2008).

We further evaluated whether the MAPK-inhibiting effects of TRF were associated with a decrease in COX-2 expression in HaCaT cells. COX-2 is an inducible enzyme involved in PGE₂ biosynthesis from arachidonic acid. HaCaT cells were pre-treated with 20 μM TRF and/or 10 μM p38 inhibitor (SB203580), JNK inhibitor (SP60012), and ERK 1/2 inhibitor (U0126) for 1 h, followed by PM_{2.5} exposure for 24 h. As Fig. 6

shows, TRF treatment and the three individual inhibitors decreased COX-2 expression following exposure to PM_{2.5}. Moreover, treatment with TRF in combination with the respective inhibitors resulted in greater COX-2 downregulation, indicating that TRF exerts anti-inflammatory effects on COX2 upon PM_{2.5} exposure via MAPK cell signalling.

Overall, these results demonstrate that TRF effectively suppressed PM_{2.5}-induced activation of the MAPK and NF-κB pathways.

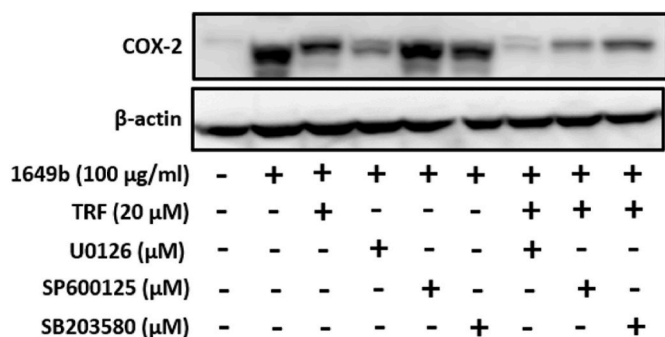


Fig. 6. COX-2 expression induced by PM2.5 reduced by treatment with TRF or/and ERK1/2, p38 and JNK1/2 inhibitors (U0126, SB203580, and SP600125 respectively) as analysed by western blotting. TRF, tocotrienol-rich fraction; αTP, MAPKs, mitogen-activated protein kinases; JNK, c-jun N-terminal kinase; ERK, extracellular signal-regulated kinase; COX-2, cyclooxygenase-2; 1649b, PM2.5 (particulate matter that has the diameter of less than 2.5 µm).

3.4. TRF restored the PM2.5-induced skin barrier impairment in HaCaT cells

Three structures maintain proper skin barrier function: the cornified envelope, corneocyte-bound lipid envelope, and intercellular space lipids. FLG and IVL are molecules that constitute the scaffold of the cornified envelope and are cross-linked by TGM-1 (Furue 2020). FLG is crucial in the skin because it is a key protein that prevents water loss and maintains the protective role of the skin. IVL, which acts as a scaffolding protein, is associated with the maintenance of epidermal barrier function. A loss in the integrity of the skin barrier allows irritants and infections to access deep layers of the skin (Hogan et al., 2012). In PM-induced human keratinocytes, increased COX-2 expression and PGE2 regulation downregulate FLG (Lee et al., 2016).

As Fig. 7 shows, PM2.5-induced HaCaT cells displayed a significant impairment of skin barrier function, as evidenced by FLG, TGM-1, and IVL levels decreasing by 40%, 33%, and 42%, respectively. According to the levels of these three biomarkers, TRF was more effective than αTP and RA in reducing PM2.5-induced skin barrier dysfunction. Notably, our results show that 1 µM RA was only effective at restoring FLG enzyme activity after PM2.5 stimulation. However, this observation was contradicted by a few studies which revealed that RA treatment significantly downregulated the levels of FLG and other skin barrier markers (Li et al., 2019; Lee 2020). Other studies have revealed that the inducing and inhibitory effects of RA are dependent on the cell type and differentiation state (Lee et al., 2009; Jean et al., 2011; Colombo et al., 2017). The disparity between our results and those of other studies could be attributed to the differences in cell differentiation state. Another study used fresh human keratinocytes (human epidermal skin cells isolated from human breast skin), whereas our study used immortalised HaCaT cells. As human keratinocytes and immortalised cells have different differentiation rates, this could have resulted in a difference in the mode of RA action. Furthermore, a review conducted in 2018 showed that reduced FLG and TGM-1 levels likely lead to skin barrier deficiencies, and IVL knockdown in mice models showed a normal skin phenotype (Egawa and Kabashima 2018). This indicates that FLG and TGM-1 are influential in maintaining skin barrier function, whereas IVL is of lesser importance.

In contrast, αTP did not significantly restore any of the three markers involved in skin barrier dysfunction. This may be due to the differences in the isoforms of vitamin E in TRF and αTP. A previous study revealed that γT3 binds to AhR, promoting and upregulating gene activity (Yamashita et al., 2016). PM and AhR interactions lead to AhR activity suppression, ultimately resulting in a decrease in the expression of skin barrier markers, such as FLG and IVL (Furue et al., 2015). Our TRF was comprised 30% γT3, and therefore, it had a higher efficiency in binding

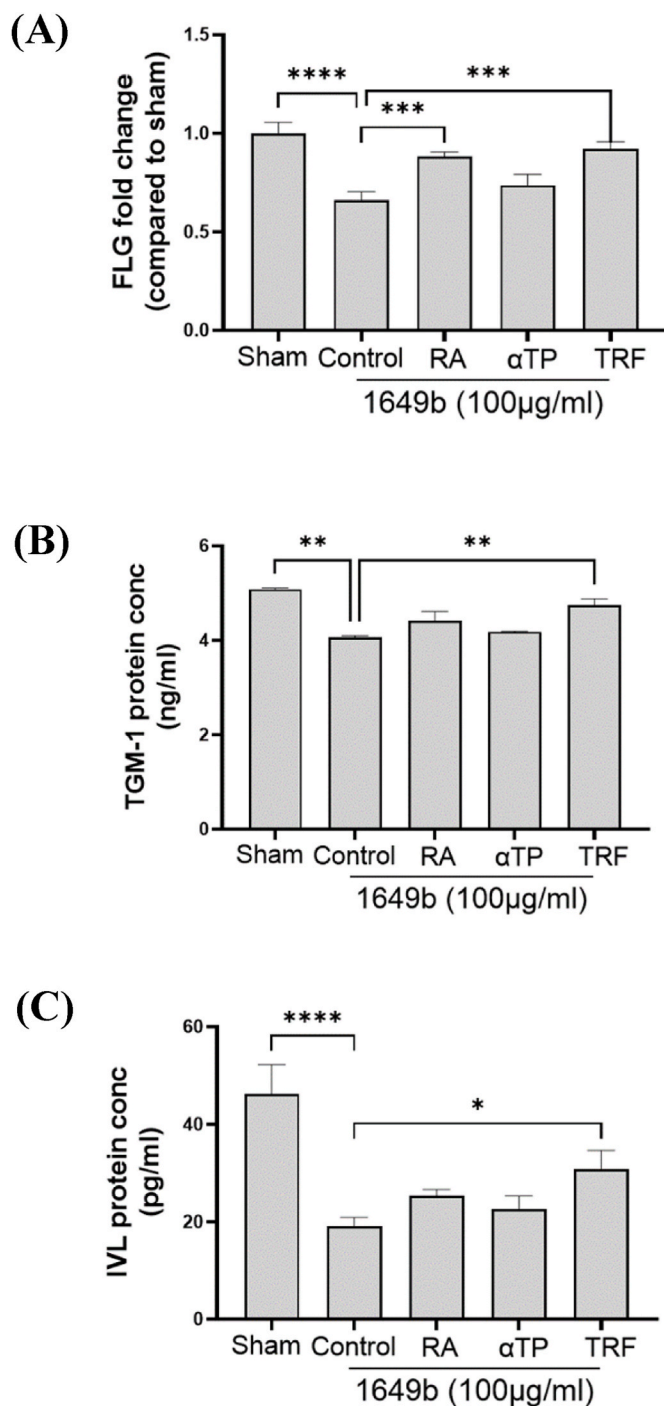


Fig. 7. Effects of TRF, αTP, and RA treatments on the skin barrier function upon PM2.5 exposure. HaCaT cells were pre-treated with TRF (20 µM) or RA (1 µM) followed by 100 µg/ml PM2.5 exposure. The cells continue with post-treatment with the individual treatments for 24 h. Cells were collected to quantify the markers of skin barrier (A) FLG; (B) TGM-1 and (C) IVL by ELISA assay according to their manufacturers' instruction. Data are expressed as mean ± standard deviation of three independent experiments. * $P < 0.05$, ** $P < 0.01$, *** $P < 0.001$ and **** $P < 0.0001$, as assessed by one-way ANOVA, followed by Tukey's post hoc test. TRF, tocotrienol-rich fraction; αTP, alpha tocopherol; RA, retinoic acid; FLG, filaggrin; TGM-1, transglutaminase-1; IVL, involucrin, IVL; 1649b, PM2.5 (particulate matter that has the diameter of less than 2.5 µm).

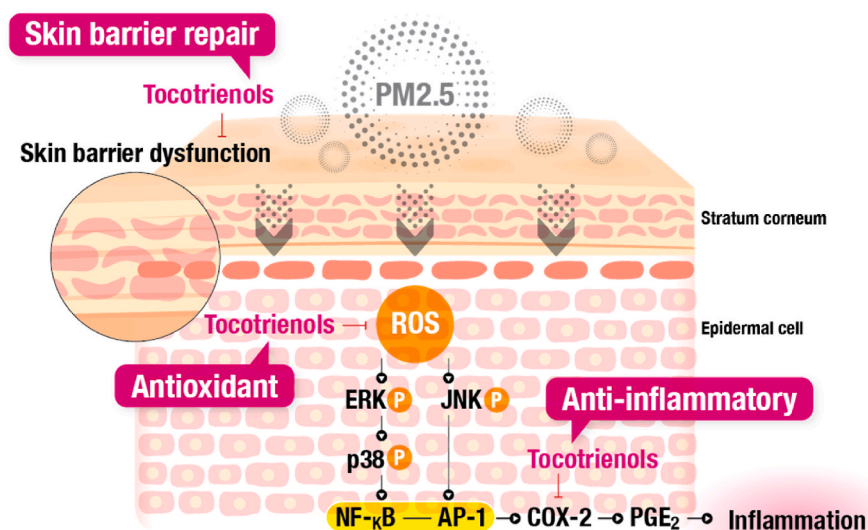


Fig. 8. Schematic diagram illustrating the proposed mechanism of TRF involved in PM_{2.5}-induced signalling pathways in HaCaT cells. TRF reduces the generation of intracellular ROS which subsequently inhibiting the 2 signalling cascades (ERK/p38-dependent activation of NF-κB and JNK-dependent activation of AP-1) in HaCaT cells upon particulate matter induction. TRF which reduces the COX-2 protein expression ameliorates skin barrier impairment as evidenced by down-regulation of FLG, TGM-1 and INV after exposed with particulate matter. TRF, tocotrienol-rich fraction; FLG, filaggrin; TGM-1, transglutaminase-1; IVL, involucrin, IVL; PM_{2.5}, particulate matter that has the diameter of less than 2.5 μm; COX-2, cyclooxygenase 2; JNK, c-jun N-terminal kinase; ERK, extracellular signal-regulated kinase; NF-κB, nuclear factor-kappa B; AP-1, activating protein-1; PGE₂, prostaglandin E₂.

to the AhR receptors but not αTP. Overall, these results suggest that T3 is a superior form of vitamin E in the gene modulation of skin, as its beneficial effects go beyond that of an antioxidant.

4. Conclusions

Our results demonstrated that PM_{2.5} induced skin damage by upregulating free radical generation, which subsequently activated the MAPKs cell signalling cascade. This, in turn, triggered inflammation and skin barrier dysfunction via FLG and COX-2 downregulation. To the best of our knowledge, this is the first study to decipher the biological functions of TRF in air pollution-induced skin damage via a combination of mechanisms, such as antioxidant, anti-inflammatory, and skin barrier function restoration (Fig. 8). TRF exhibited superior protective effects compared with αTP and RA. In conclusion, TRF can be considered as a potential natural active ingredient that can protect against PM_{2.5}-induced skin ageing in the cosmeceutical and nutraceutical industries.

Credit author statement

Juvenia Rui En Neo: Revision, Investigation, Formal analysis, Project Administration, Writing- Review & Editing; **Zi Ning Teo:** Investigation, Formal analysis, Project Administration, Writing- original draft; **Jolene Shi En Yeo:** Investigation, Project Administration, Formal analysis; **Cassey Kai Sing Ng:** Investigation, Formal analysis, Project Administration; **Cheryl Wei Ling Teo:** Project Administration; **Yee Wei Ung:** Conceptualization, Writing- Review & Editing; **Wei Ney Yap:** Conceptualization, Supervision, Validation, Writing- Review & Editing.

Funding

This work was supported financially by a research fund from KL-Kepong Oleomas (KLK Oleo) to Davos Life Science Pte Ltd.

Declaration of competing interest

The authors declare the following financial interests/personal relationships which may be considered as potential competing interests: Wei Ney Yap reports financial support was provided by Klk Oleo Sdn Bhd. Wei Ney Yap reports a relationship with Klk Oleo Sdn Bhd that includes: employment. Juvenia Rui En Neo reports a relationship with Klk Oleo Sdn Bhd that includes: employment. Yee Wei Ung reports a

relationship with Klk Oleo Sdn Bhd that includes: employment. Cheryl Wei Ling Teo reports a relationship with Klk Oleo Sdn Bhd that includes: employment.

Acknowledgements

The authors extend special thanks to Associate Professor Dr Gautham Sethi for the HaCaT cells and Mr Vincent Boey Ying Shiun for the graphical abstract.

References

- Agency, U.S.E.P., 2020. Particulate matter (PM) basics. from. <https://www.epa.gov/pm-pollution/particulate-matter-pm-basics>.
- Aggarwal, V., Kashyap, D., Sak, K., Tuli, H.S., Jain, A., Chaudhary, A., Garg, V.K., Sethi, G., Yerer, M.B., 2019. Molecular mechanisms of action of tocotrienols in cancer: recent trends and advancements. *Int. J. Mol. Sci.* 20 (3).
- Ahsan, H., Ahad, A., Iqbal, J., Siddiqui, W.A., 2014. Pharmacological potential of tocotrienols: a review. *Nutr. Metab.* 11 (1), 52.
- Azzi, A., 2007. Molecular mechanism of alpha-tocopherol action. *Free Radic. Biol. Med.* 43 (1), 16–21.
- Brand-Williams, W., Cuvelier, M.E., Berset, C., 1995. Use of a free radical method to evaluate antioxidant activity. *Food Sci Tech* 28 (1), 25–30.
- Byrd, A.L., Belkaid, Y., Segre, J.A., 2018. The human skin microbiome. *Nat. Rev. Microbiol.* 16 (3), 143–155.
- Colombo, I., Sangiovanni, E., Maggio, R., Mattozzi, C., Zava, S., Corbett, Y., Fumagalli, M., Carlino, C., Corsetto, P.A., Scaccabarozzi, D., Calvieri, S., Gismondi, A., Taramelli, D., Dell'Agli, M., 2017. HaCaT cells as a reliable in vitro differentiation model to dissect the inflammatory/repair response of human keratinocytes. *Mediat. Inflamm.*, 7435621, 2017.
- Dijkhoff, I.M., Drasler, B., Karakocak, B.B., Petri-Fink, A., Valacchi, G., Eeman, M., Rothen-Rutishauser, B., 2020. Impact of airborne particulate matter on skin: a systematic review from epidemiology to in vitro studies. *Part. Fibre Toxicol.* 17 (1), 35.
- Egawa, G., Kabashima, K., 2018. Barrier dysfunction in the skin allergy. *Allergol. Int.* 67 (1), 3–11.
- Fu, H., Yen, F.L., Huang, P.H., Yang, C.Y., Yen, C.H., 2021. Oleonic acid nanofibers attenuated particulate matter-induced oxidative stress in keratinocytes. *Antioxidants* 10 (9).
- Furue, M., 2020. Regulation of filaggrin, loricrin, and involucrin by IL-4, IL-13, IL-17a, IL-22, AHR, and NRF2: pathogenic implications in atopic dermatitis. *Int. J. Mol. Sci.* 21 (15).
- Furue, M., Tsuji, G., Mitoma, C., Nakahara, T., Chiba, T., Morino-Koga, S., Uchi, H., 2015. Gene regulation of filaggrin and other skin barrier proteins via aryl hydrocarbon receptor. *J. Dermatol. Sci.* 80 (2), 83–88.
- Gulcin, I., 2020. Antioxidants and antioxidant methods: an updated overview. *Arch. Toxicol.* 94 (3), 651–715.
- Hogan, M.B., Peele, K., Wilson, N.W., 2012. Skin barrier function and its importance at the start of the atopic march. *J Allergy (Cairo)*, 901940, 2012.
- Huang, P.H., Tseng, C.H., Lin, C.Y., Lee, C.W., Yen, F.L., 2018. Preparation, characterizations and anti-pollutant activity of 7,3',4'-trihydroxyisoflavone

- nanoparticles in particulate matter-induced HaCaT keratinocytes. *Int. J. Nanomed.* 13, 3279–3293.
- Jean, J., Soucy, J., Pouliot, R., 2011. Effects of retinoic acid on keratinocyte proliferation and differentiation in a psoriatic skin model. *Tissue Eng.* 17 (13–14), 1859–1868.
- Jiang, Q., Yin, X., Lill, M.A., Danielson, M.L., Freiser, H., Huang, J., 2008. Long-chain carboxychromanols, metabolites of vitamin E, are potent inhibitors of cyclooxygenases. *Proc. Natl. Acad. Sci. U. S. A.* 105 (51), 20464–20469.
- Kim, K.E., Cho, D., Park, H.J., 2016. Air pollution and skin diseases: adverse effects of airborne particulate matter on various skin diseases. *Life Sci.* 152, 126–134.
- Kim, Y.M., Kim, J., Ha, S.C., Ahn, K., 2021. Effects of exposure to indoor fine particulate matter on atopic dermatitis in children. *Int. J. Environ. Res. Publ. Health* 18 (21).
- Kloog, I., Ridgway, B., Koutrakis, P., Coull, B.A., Schwartz, J.D., 2013. Long- and short-term exposure to PM_{2.5} and mortality: using novel exposure models. *Epidemiology* 24 (4), 555–561.
- Lee, A.Y., 2020. Molecular mechanism of epidermal barrier dysfunction as primary abnormalities. *Int. J. Mol. Sci.* 21 (4).
- Lee, C.W., Lin, Z.C., Hu, S.C., Chiang, Y.C., Hsu, L.F., Lin, Y.C., Lee, I.T., Tsai, M.H., Fang, J.Y., 2016. Urban particulate matter down-regulates filaggrin via COX2 expression/PGE2 production leading to skin barrier dysfunction. *Sci. Rep.* 6, 27995.
- Lee, D.D., Stojadinovic, O., Krzyzanowska, A., Vouthounis, C., Blumenberg, M., Tomic-Canic, M., 2009. Retinoid-responsive transcriptional changes in epidermal keratinocytes. *J. Cell. Physiol.* 220 (2), 427–439.
- Li, J., Li, Q., Geng, S., 2019. Alltrans retinoic acid alters the expression of the tight junction proteins Claudin1 and 4 and epidermal barrier function-associated genes in the epidermis. *Int. J. Mol. Med.* 43 (4), 1789–1805.
- Liu, W., Huang, S., Li, Y., Li, Y., Li, D., Wu, P., Wang, Q., Zheng, X., Zhang, K., 2018. Glycyrrhizic acid from licorice down-regulates inflammatory responses via blocking MAPK and PI3K/Akt-dependent NF- κ B signalling pathways in TPA-induced skin inflammation. *Medchemcomm* 9 (9), 1502–1510.
- Liu, X., Yang, G., Luo, M., Lan, Q., Shi, X., Deng, H., Wang, N., Xu, X., Zhang, C., 2021. Serum vitamin E levels and chronic inflammatory skin diseases: a systematic review and meta-analysis. *PLoS One* 16 (12), e0261259.
- Loxham, M., Davies, D.E., Holgate, S.T., 2019. The health effects of fine particulate air pollution. *BMJ* 367, 16609.
- Marengo, B., Nitti, M., Furfaro, A.L., Colla, R., Ciucis, C.D., Marinari, U.M., Pronzato, M. A., Traverso, N., Domenicotti, C., 2016. Redox homeostasis and cellular antioxidant systems: crucial players in cancer growth and therapy. *Oxid. Med. Cell. Longev.*, 6235641, 2016.
- Marill, J., Idres, N., Capron, C.C., Nguyen, E., Chabot, G.G., 2003. Retinoic acid metabolism and mechanism of action: a review. *Curr. Drug Metabol.* 4 (1), 1–10.
- Mohd Zaffarin, A.S., Ng, S.F., Ng, M.H., Hassan, H., Alias, E., 2020. Pharmacology and pharmacokinetics of vitamin E: nanoformulations to enhance bioavailability. *Int. J. Nanomed.* 15, 9961–9974.
- Ngoc, L.T.N., Park, D., Lee, Y., Lee, Y.C., 2017. Systematic review and meta-analysis of human skin diseases due to particulate matter. *Int. J. Environ. Res. Publ. Health* 14 (12).
- Nguyen, A.V., Soulika, A.M., 2019. The dynamics of the skin's immune system. *Int. J. Mol. Sci.* 20 (8).
- Niki, E., 2015. Lipid oxidation in the skin. *Free Radic. Res.* 49 (7), 827–834.
- Oliveira, L.M., Teixeira, F.M.E., Sato, M.N., 2018. Impact of retinoic acid on immune cells and inflammatory diseases. *Mediat. Inflamm.*, 3067126, 2018.
- Organization, W. H. "Air pollution." Retrieved 29/2, 2021, from <https://www.who.int/news-room/air-pollution>.
- Peh, H.Y., Tan, W.S., Liao, W., Wong, W.S., 2016. Vitamin E therapy beyond cancer: tocopherol versus tocotrienol. *Pharmacol. Ther.* 162, 152–169.
- Piao, M.J., Ahn, M.J., Kang, K.A., Ryu, Y.S., Hyun, Y.J., Shilnikova, K., Zhen, A.X., Jeong, J.W., Choi, Y.H., Kang, H.K., Koh, Y.S., Hyun, J.W., 2018. Particulate matter 2.5 damages skin cells by inducing oxidative stress, subcellular organelle dysfunction, and apoptosis. *Arch. Toxicol.* 92 (6), 2077–2091.
- Rinnerthaler, M., Bischof, J., Streubel, M.K., Trost, A., Richter, K., 2015. Oxidative stress in aging human skin. *Biomolecules* 5 (2), 545–589.
- Shi, Y., Zeng, Z., Liu, J., Pi, Z., Zou, P., Deng, Q., Ma, X., Qiao, F., Xiong, W., Zhou, C., Zeng, Q., Xiao, R., 2021. Particulate matter promotes hyperpigmentation via AhR/MAPK signaling activation and by increasing alpha-MSH paracrine levels in keratinocytes. *Environ. Pollut.* 278, 116850.
- Sirivibulkovit, K., Nouanthavong, S., Samenoi, Y., 2018. Paper-based DPPH assay for antioxidant activity analysis. *Anal. Sci.* 34 (7), 795–800.
- Szymanski, L., Skopek, R., Palusinska, M., Schenk, T., Stengel, S., Lewicki, S., Kraj, L., Kaminski, P., Zelent, A., 2020. Retinoic acid and its derivatives in skin. *Cells* 9 (12).
- Ungurianu, A., Zandfirescu, A., Nitulescu, G., Margina, D., 2021. Vitamin E beyond its antioxidant label. *Antioxidants* 10 (5).
- Wong, S.K., Kamisah, Y., Mohamed, N., Muhammad, N., Masbah, N., Fahami, N.A.M., Mohamed, I.N., Shuid, A.N., Saad, Q.M., Abdullah, A., Mohamad, N.V., Ibrahim, N. I., Pang, K.L., Chow, Y.Y., Thong, B.K.S., Subramaniam, S., Chan, C.Y., Ima-Nirwana, S., Chin, A.K., 2020. Potential role of tocotrienols on non-communicable diseases: a review of current evidence. *Nutrients* 12 (1).
- Wu, S.J., Liu, P.L., Ng, L.T., 2008. Tocotrienol-rich fraction of palm oil exhibits anti-inflammatory property by suppressing the expression of inflammatory mediators in human monocytic cells. *Mol. Nutr. Food Res.* 52 (8), 921–929.
- Yamashita, S., Baba, K., Makio, A., Kumazoe, M., Huang, Y., Lin, I.C., Bae, J., Murata, M., Yamada, S., Tachibana, H., 2016. gamma-Tocotrienol upregulates aryl hydrocarbon receptor expression and enhances the anticancer effect of baicalein. *Biochem. Biophys. Res. Commun.* 473 (4), 801–807.
- Yang, L., Zhang, H., Zhang, X., Xing, W., Wang, Y., Bai, P., Zhang, L., Hayakawa, K., Toriba, A., Tang, N., 2021. Exposure to atmospheric particulate matter-bound polycyclic aromatic hydrocarbons and their health effects: a review. *Int. J. Environ. Res. Publ. Health* 18 (4).
- Zhang, W., Liu, H.T., 2002. MAPK signal pathways in the regulation of cell proliferation in mammalian cells. *Cell Res.* 12 (1), 9–18.
- Zhen, A.X., Hyun, Y.J., Piao, M.J., Fernando, P., Kang, K.A., Ahn, M.J., Yi, J.M., Kang, H. K., Koh, Y.S., Lee, N.H., Hyun, J.W., 2019. Eckol inhibits particulate matter 2.5-induced skin keratinocyte damage via MAPK signaling pathway. *Mar. Drugs* 17 (8).



Article

Tocotrienol-Rich Fraction Attenuates Blue Light-Induced Oxidative Stress and Melanogenesis in B16-F1 Melanocytes via Anti-Oxidative and Anti-Tyrosinase Properties

Juvenia Rui En Neo¹, Cheryl Wei Ling Teo¹, Yee Wei Ung² and Wei Ney Yap^{1,*}

¹ Research and Development Department, Davos Life Science, 3 Biopolis Drive, #04-19 Synapse, Singapore 138623, Singapore; ruien.neo@davoslife.com (J.R.E.N.); weiling3944@gmail.com (C.W.L.T.)

² Research and Development Department, KL-Kepong Oleomas (KLK Oleo), Level 8, Menara KLK, No 1, Jalan PJU 7/6, Mutiara Damansara, Petaling Jaya 47810, Malaysia; yw.ung@klkoleo.com

* Correspondence: weiney.yap@davoslife.com; Tel.: +65-65139388; Fax: +65-68629023

Abstract: Our skin is constantly exposed to blue light (BL), which is abundant in sunlight and emitted by digital devices. Prolonged exposure to BL can lead to oxidative stress-induced damages and skin hyperpigmentation. For this study, we used a cell line-based model to examine the protective effects of tocotrienol-rich fraction (TRF) on BL-induced oxidative stress and hyperpigmentation in B16-F1 melanocytes. Alpha-tocopherol (α TP) was used as a comparator. Molecular assays such as cell viability assay, flow cytometry, western blotting, fluorescence imaging, melanin and tyrosinase analysis were performed. Our results showed that TRF effectively suppressed the formation of reactive oxygen species and preserved the mitochondrial membrane potential. Additionally, TRF exhibited anti-apoptotic properties by reducing the activation of the p38 mitogen-activated protein kinase molecule and downregulating the expression of cleaved caspase-3. Moreover, TRF modulated tyrosinase activity, resulting in a lowered rate of melanogenesis and reduced melanin production. In contrast, α TP did not exhibit significant protective effects against skin damages and pigmentation in BL-induced B16-F1 cells. Therefore, this study indicates that TRF may offer superior protective effects over α TP against the effects of BL on melanocytes. These findings demonstrate the potential of TRF as a protective natural ingredient that acts against BL-induced skin damages and hyperpigmentation via its anti-oxidative and anti-melanogenic properties.

Keywords: blue light; oxidative stress; pigmentation; tocotrienol-rich fraction; anti-oxidant; anti-melanogenesis; melanocyte



Citation: Neo, J.R.E.; Teo, C.W.L.; Ung, Y.W.; Yap, W.N. Tocotrienol-Rich Fraction Attenuates Blue Light-Induced Oxidative Stress and Melanogenesis in B16-F1 Melanocytes via Anti-Oxidative and Anti-Tyrosinase Properties. *Int. J. Mol. Sci.* **2023**, *24*, 15373. <https://doi.org/10.3390/ijms242015373>

Academic Editor: Ji Hyun Lee

Received: 22 September 2023

Revised: 14 October 2023

Accepted: 18 October 2023

Published: 19 October 2023



Copyright: © 2023 by the authors. Licensee MDPI, Basel, Switzerland. This article is an open access article distributed under the terms and conditions of the Creative Commons Attribution (CC BY) license (<https://creativecommons.org/licenses/by/4.0/>).

1. Introduction

Our skin acts as a crucial barrier between the body and the external environment, protecting it from various environmental factors such as solar radiation and air pollution [1]. It serves as the primary defence and repair mechanism for the body while also contributing to the maintenance of normal homeostasis. It is made up of three layers: the epidermis, dermis, and subcutaneous tissue. Melanocytes, which are located in the basal layer of the epidermis, are an integral type of skin cell. These specialized cells synthesize melanin through a complex enzymatic process that gives rise to skin, eye, and hair colour in humans and animals [2,3]. Sunlight, which is essential for the survival of most living organisms, consists of a range of wavelengths. The solar spectrum includes ultra-violet (UV) rays, visible light, and infrared rays, that enter the terrestrial environment. Among these, UV rays comprise only 2% of the solar spectrum, while visible light and infrared rays account for nearly half of the solar spectrum [4]. Numerous studies have focused on understanding the skin protective measures required to fight against UV rays, as they have the shortest wavelength (100 to 400 nm) and more energy compared to visible light (400 to 780 nm) and infrared rays (780 to 3000 nm), which have longer wavelengths and less energy [5]. Despite

having less energy, visible light is known to penetrate deeper into the skin due to its longer wavelength. The visible light spectrum consists of various colours, including (increasing order of wavelengths) violet, blue, green, yellow, orange, and red light. Blue light (BL; 450 to 485 nm) is one of the most extensively studied visible light wavelengths [4]. BL can be found in sunlight and artificially in devices such as light-emitting diode (LED) screens (laptop, mobile, and tablet screens) or compact fluorescent lamp devices [6]. Recent studies have shown that BL can have detrimental effects on the skin, including the induction of skin pigmentation and photoaging [7,8]. BL has also been extensively studied for its potential in phototherapy against skin diseases such as melanoma as it can slow cell growth and promote apoptosis in melanoma cells. These effects are attributed to the accumulation of reactive oxygen species (ROS) molecules such as superoxide, which can lead to mitochondrial membrane alterations and cell death [9,10]. As such, prolonged exposure to BL on healthy skin may result in irreversible damage to the skin. Therefore, it is widely acknowledged that exposure to artificial BL in modern times may have detrimental effects on skin health, leading to oxidative stress and pigmentation. Consequently, further studies are necessary to investigate the measures for protecting melanocytes against the damaging effects of BL.

In such circumstances, anti-oxidants can effectively prevent damage caused by oxidative stress by maintaining a balanced cellular redox environment [11]. Vitamin E has a well-established history of use in dermatology, cardiovascular health, and neuroprotection due to its potent anti-oxidant and anti-inflammatory properties. It can be found in various food sources, such as plant oils and seeds [12]. Studies have shown that vitamin E can alleviate inflammatory skin diseases and provide significant photoprotective effects [13,14]. Vitamin E primarily exists in eight isoforms, including α -, β -, γ -, and δ -tocopherol (TP) and α -, β -, γ -, and δ -tocotrienol (T3). Both TPs and T3s differ in terms of their structural form, where T3s have the presence of an unsaturated side chain that enables better penetration into fatty tissues, making them more potent anti-oxidants compared to TPs [15]. T3s have also been shown to protect the skin from oxidative stress-induced damage caused by particulate matter and exhibit whitening effect by suppressing tyrosinase activity in UV-induced melanocytes, as reported in our previous studies [16,17]. In this study, we investigated the protective effects of T3s against the harmful effects of prolonged BL exposure on murine melanoma cells B16-F1. Our study involved using tocotrienol-rich fraction (TRF), which comprises four T3 isoforms (α -, β -, γ -, and δ -T3s) and α TP. The other vitamin E comparator used in this study was α TP, a commonly abundant form of vitamin E in the body [15]. Although several studies have investigated the benefits of T3s for skin health, there is a lack of studies specifically focused on the effects of T3s on prolonged BL exposure. Given the potent anti-oxidative activities of T3s, it is hypothesized that T3s can protect the skin from excessive ROS generation, thereby alleviating cell death and skin hyperpigmentation. Therefore, our study aimed to elucidate the protective effects of T3s against BL exposure by investigating the anti-oxidative and anti-pigmentating mechanisms. To achieve this, the effects of TRF on BL-induced melanocytes were examined through a cell viability assay. Subsequent experiments revealed the presence of apoptosis, ROS formation, mitochondria damage, an increase in melanin levels, and elevated tyrosinase activity induced by BL. Additionally, an upregulation of activated p38 mitogen-activated protein kinases (MAPK) and cleaved caspase-3 protein were observed. Collectively, these results illustrate the protective abilities of TRF against BL-induced damage and pigmentation in melanocytes.

2. Results

2.1. TRF Improved Cell Viability of BL-Induced Melanocytes

The 3-[4,5-dimethylthiazol-2-yl]-2,5-diphenyltetrazoliumbromide (MTT) assay was used to assess cell proliferation. To determine the optimal dosage of BL exposure for the cells, we performed cell irradiation at three different time points—1 h (12 J/cm²), 2 h (25 J/cm²), and 3 h (38 J/cm²)—using an MTT assay. Our results show a dose-dependent decrease in cell viability, with no significant difference between 25 and 38 J/cm² (Figure 1A).

Thus, 38 J/cm^2 was selected for our experiment to better represent real-life BL exposure. This dosage is equivalent to approximately 300 h of BL exposure from electronic devices at 100% screen brightness [18]. Additionally, a previous study indicated that this dosage induced minimal lethal oxidative stress in cells, making it suitable for accurate experimentation [7]. We further assessed the effect of TRF on cell viability and found that treatment with $20 \mu\text{M}$ of TRF significantly increased the cell viability of BL-treated B16-F1 cells compared to αTP , where only a modest increase was observed (Figure 1B).

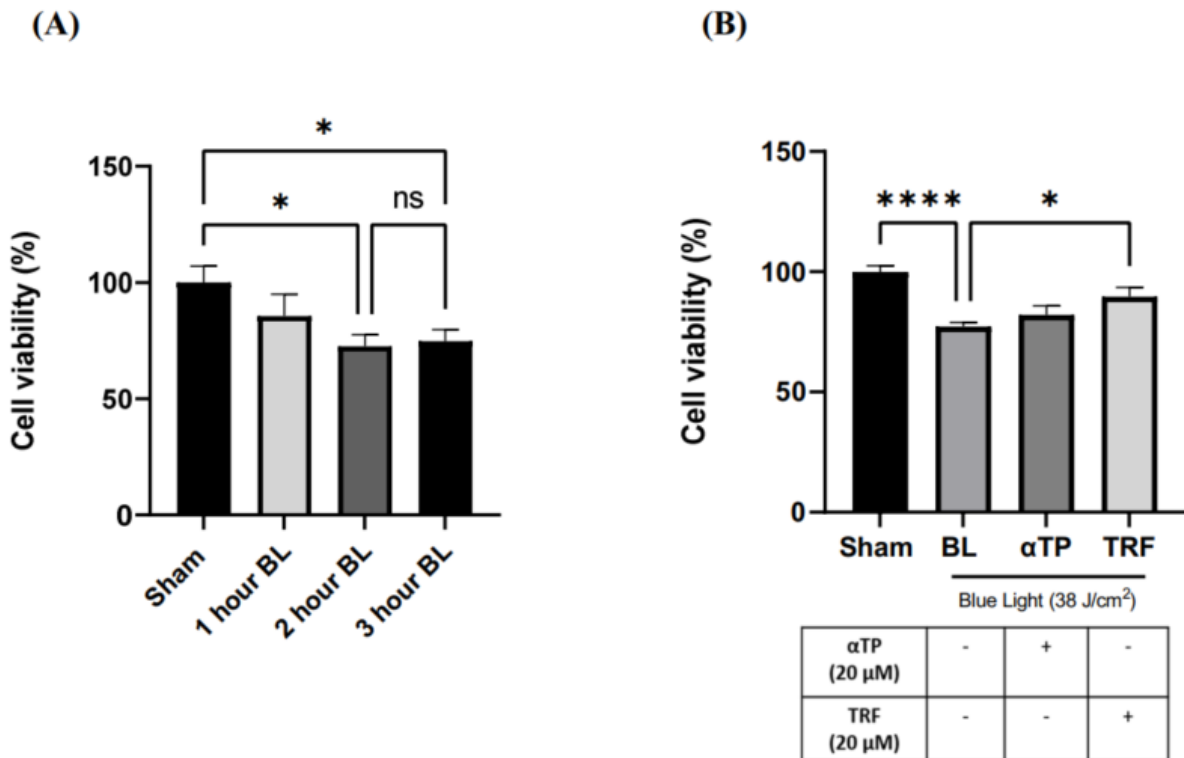


Figure 1. Cell viability of B16-F1 was evaluated via MTT assay 24 h after BL exposure and treatment. (A) Measurement of B16-F1 cell viability exposed with different dosages of BL. (B) Measurement of B16-F1 cell viability induced with BL, accompanied with αTP or TRF treatment. Data shown are expressed as % of sham and expressed as mean \pm standard error of the mean (SEM). **** $p < 0.0001$ and * $p < 0.05$ indicate statistical significance. ns indicates no statistical significance.

2.2. TRF Inhibited BL-Induced Cell Apoptosis

Based on the findings presented in Section 2.1, our study aimed to investigate the level of apoptosis in B16-F1 cells following exposure to blue light. To provide further evidence supporting our findings, we conducted a flow cytometry assay to assess the population of apoptotic cells in both BL-induced/treated groups. A previous study showed that BL induced cellular apoptosis as observed in the B16-F10 cells [9]. In our study, we used an Annexin V/Propidium Iodide (PI) double-staining assay to measure the population of apoptotic and necrotic cells. Our results showed a significant increase in the population of total apoptotic cells, particularly in the early apoptotic group, in the BL-induced melanocytes (Figure 2A). Notably, the cells treated with TRF exhibited a rescue effect, as the number of apoptotic cells were significantly lower compared to the BL-irradiated cells (Figure 2B).

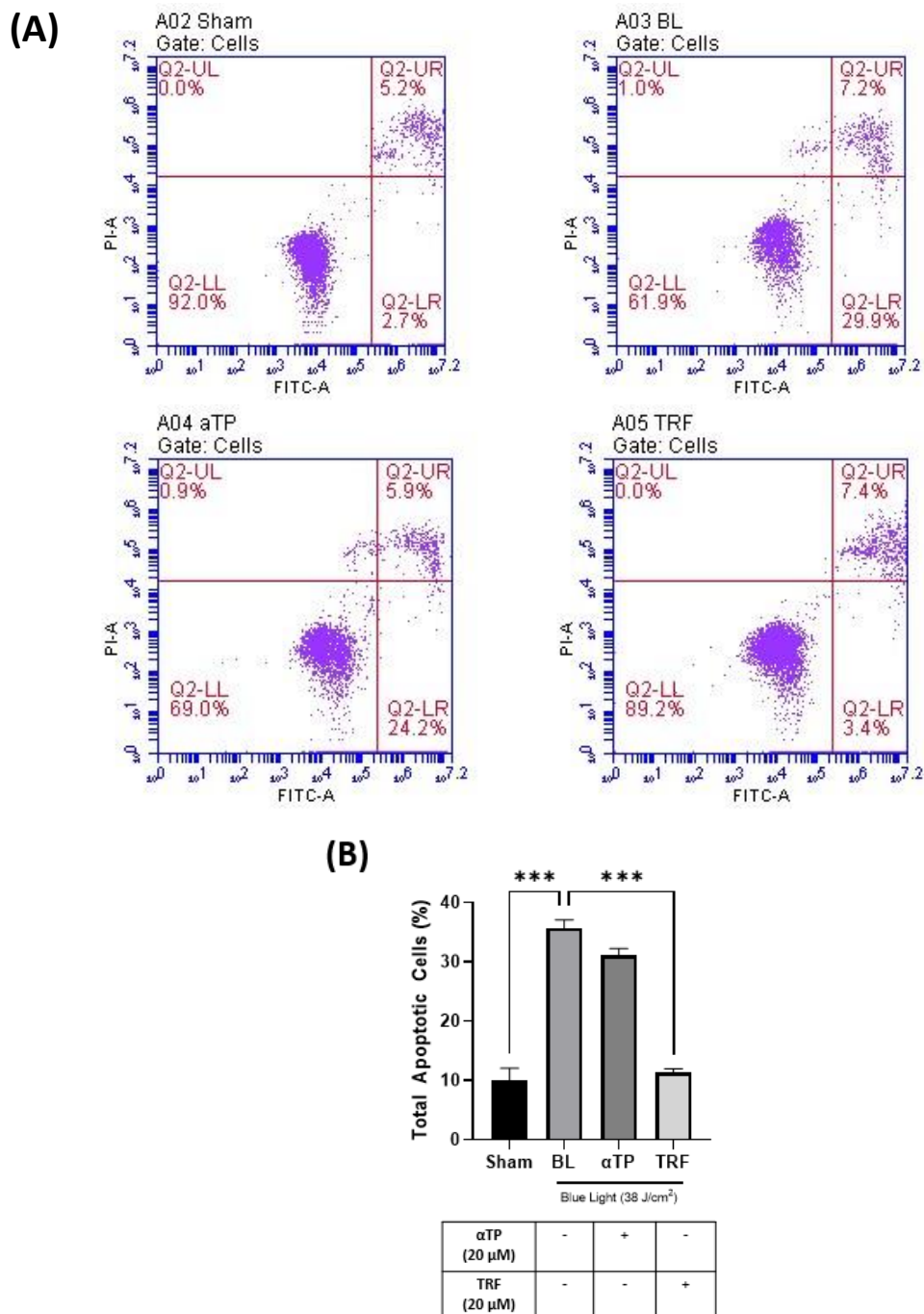


Figure 2. Flow cytometry assay of B16-F1 cells induced with BL and treatment. **(A)** Population of healthy (Q2-LL), early apoptotic (Q2-LR), late apoptotic (Q2-UR), and necrotic cells (Q2-UL) in BL-induced B16-F1 cells with designated treatment. **(B)** Total apoptotic B16-F1 cells as measured based on the early and late apoptotic populations. Data shown are expressed as % of sham and expressed as mean ± SEM. *** $p < 0.001$ indicates statistical significance.

2.3. TRF Exhibited Anti-Oxidative Effects against Oxidative Stress Induced by BL

Based on the findings presented in Sections 2.1 and 2.2, we aimed to further investigate the presence of ROS in the cells, as they may have played a significant role in the induction of apoptosis. To examine the presence of oxidative stress in B16-F1 cells exposed to blue light, we used the 2', 7'-dichlorofluorescein diacetate (DCFDA) fluorescent probe and captured images using fluorescence microscopy. We observed a stronger fluorescence signal in the cells irradiated with BL compared to the sham group (negative control group).

However, treatment with α TP and TRF resulted in a reduction in the fluorescence signal, with TRF demonstrating a higher degree of reduction (Figure 3A). To determine the levels of intracellular ROS, we measured the fluorescence intensity and normalized it to the sham group. Both treatments showed protection against ROS, with TRF showing a higher anti-oxidative capacity compared to α TP (Figure 3B).

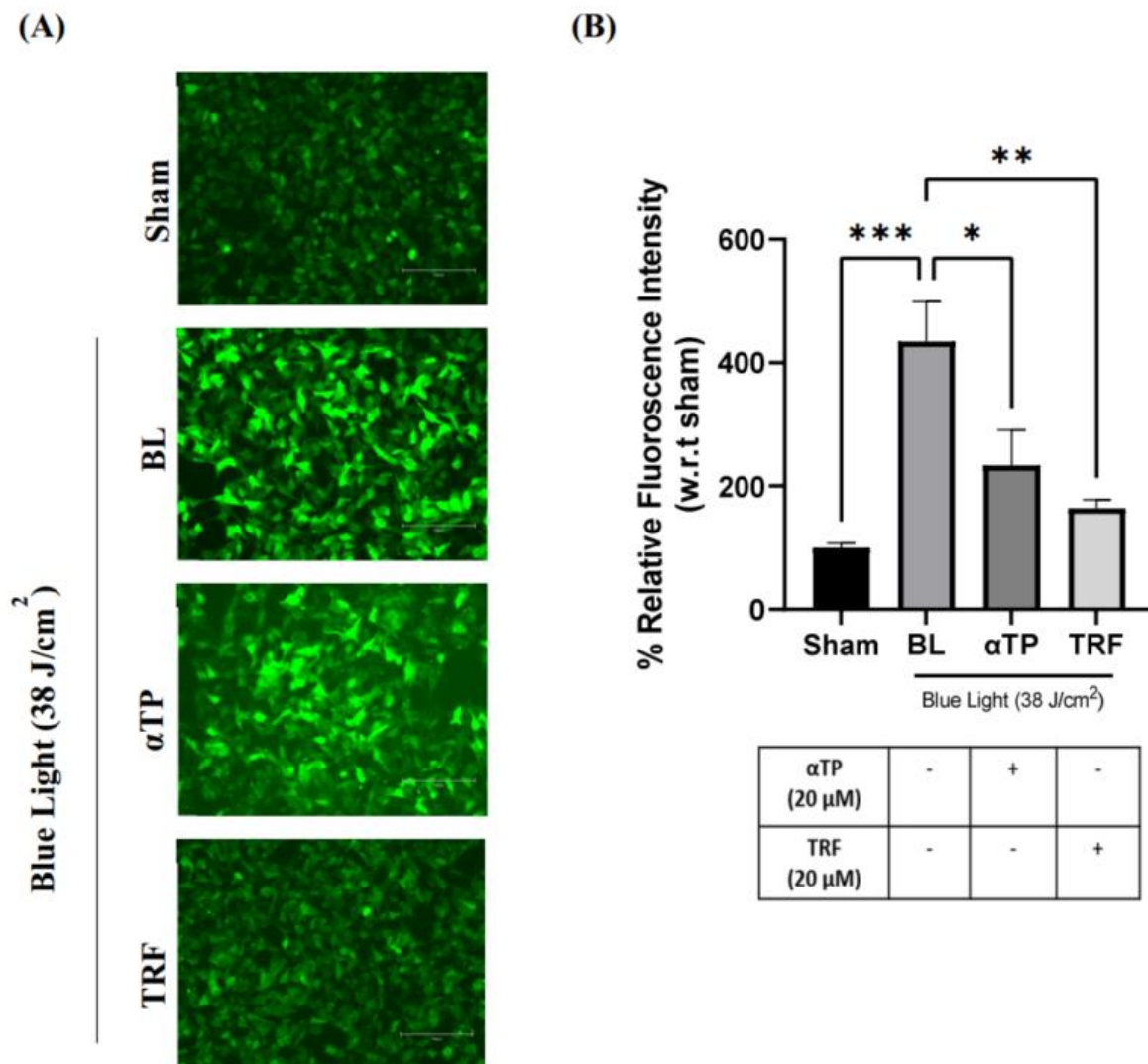


Figure 3. Presence of oxidative stress in B16-F1 melanocytes exposed to BL and treatment. (A) Fluorescence images of DCFDA as depicted by the green fluorescence. (B) Quantification of relative DCFDA fluorescence to represent intracellular ROS. Data shown are expressed as % of sham and expressed as mean \pm SEM. *** $p < 0.001$, ** $p < 0.01$, and * $p < 0.05$ represent statistical significance. Scale bar: 100 μ M.

2.4. TRF Regulated BL-Induced Mitochondrial Membrane Potential Alterations

The presence of ROS in the cells could potentially compromise important cellular organelles such as the mitochondria. To assess the mitochondrial membrane potential, we utilized the JC-1 mitochondria staining kit. The presence of JC-1 monomers is indicated by green fluorescence and indicates a healthy mitochondrion, while the presence of JC-1 aggregates, represented by red fluorescence, indicates an unhealthy mitochondrion. Therefore, the ratio of red to green fluorescence can serve as an indicator of the membrane potential [19]. Upon BL induction, a stronger intensity of green fluorescence was observed compared to red fluorescence. However, treatment with TRF exhibited a rescuing effect on the mitochondrial membrane potential, as evidenced by a significant restoration of

the ratio of red to green fluorescence (Figure 4A). As shown in Figure 4B, there was a significant reduction in the red/green fluorescence ratio following BL exposure, suggesting mitochondrial membrane depolarization. The ratio significantly improved back to baseline with TRF treatment, while this effect was not observed in the α TP group.

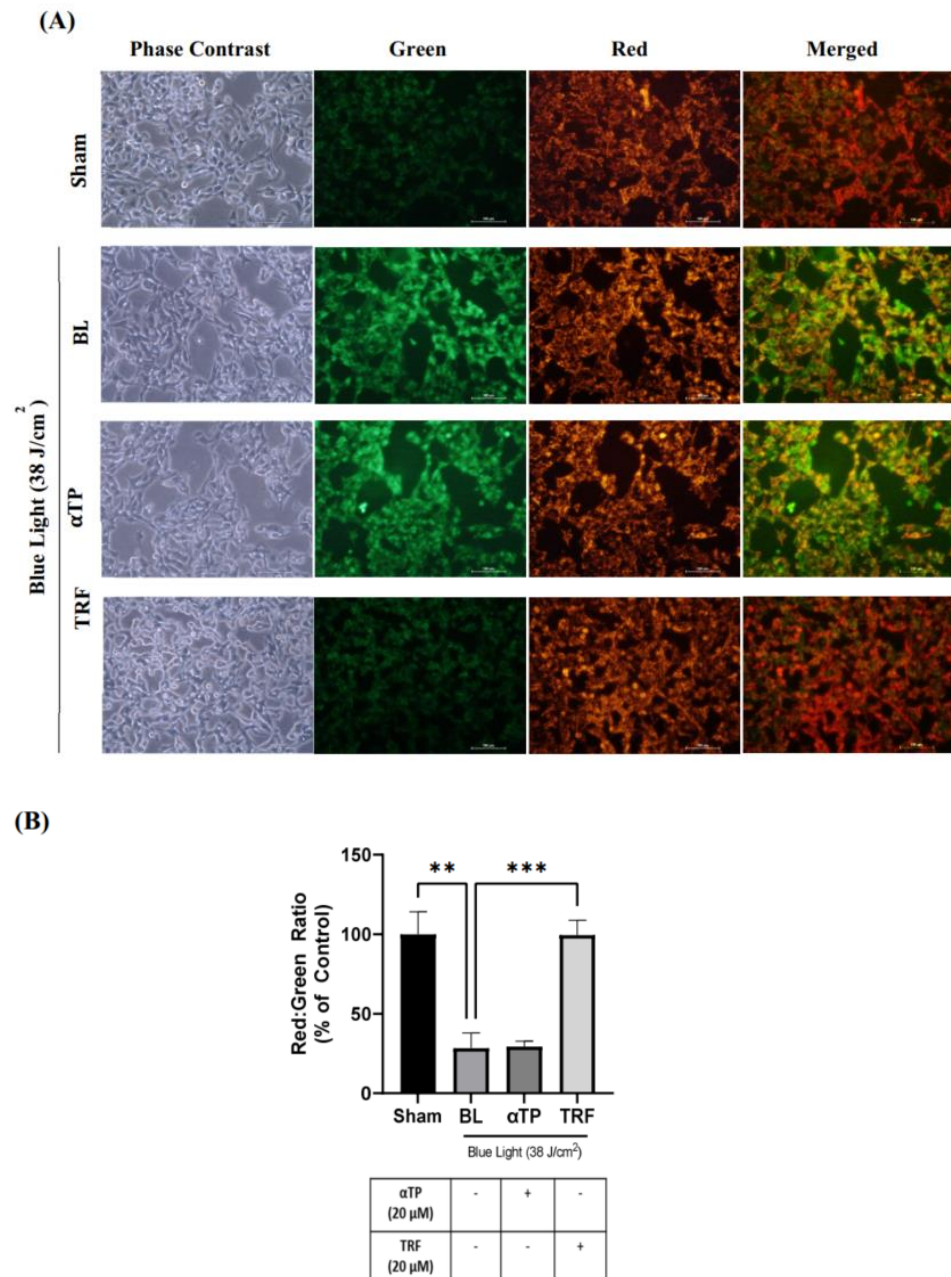


Figure 4. Mitochondrial membrane potential of B16-F1 melanocytes exposed to BL and treatments. (A) Fluorescence images of JC-1 dye. (B) Quantification of red/green fluorescence ratio to represent the polarization of the membrane potential. Data shown are expressed as % of sham and expressed as mean \pm SEM. *** $p < 0.001$ and ** $p < 0.01$ represent statistical significance. Scale bar: 100 μ M.

2.5. TRF Attenuated Cellular Death through Modulation of p38-MAPK Regulated Mitochondrial Apoptotic Pathway

Based on the results presented in Sections 2.2 and 2.4, it can be theorized that mitochondrial dysfunction induced by BL may contribute to the observed cellular death. To understand the molecular mechanisms underlying this phenomenon, we studied the expression of proteins involved in the p38-MAPK regulated mitochondrial apoptotic pathway,

namely p38 and caspase-3 [20]. Upon BL induction, there was an extensive activation of p38, as evidenced by increased phosphorylation. However, treatment with α TP and TRF resulted in a significant reduction in the levels of phosphorylated p38 (Figure 5A).

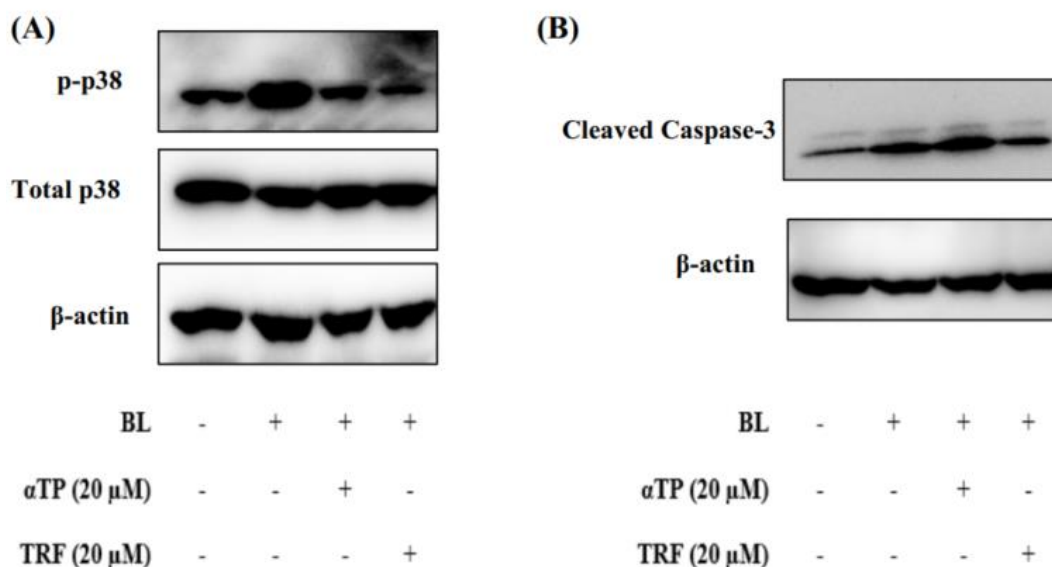


Figure 5. Protective effects of TRF against BL-induced p38 MAPK regulated mitochondrial apoptotic pathway. (A) Western blot analysis of p38 MAPK protein expression in BL exposed cells. (B) Western blot analysis showing activation of apoptotic marker upon BL induction.

Additionally, we also investigated the expression levels of caspase-3 in B16-F1 cells exposed to BL. The activation of procaspase-3, indicated by the presence of cleaved caspase-3, was observed. Notably, treatment with TRF, but not α TP, significantly decreased the levels of cleaved caspase-3 (Figure 5B). These results align with the results obtained from the Annexin-V/PI and JC-1 assays, suggesting that TRF may protect the cells from mitochondria-mediated apoptosis by preserving the mitochondrial membrane potential.

2.6. TRF Prevented Pigmentation Induced by BL through Regulation of Tyrosinase Activity

To study the effect of BL on pigmentation and the rate of melanogenesis in B16-F1 cells, we conducted a melanin assay and measured tyrosinase activity. The pigmentation effect of BL on the B16-F1 cells was investigated by observing changes in cell pellet colour and measuring intracellular and extracellular melanin content. BL exposure induced a visible darkening of the cell pellets, which was reversed by treatment with TRF (Figure 6A). This finding was corroborated by the quantification of intra- and extracellular melanin levels, which showed a significant reduction in melanin levels in the TRF-treated groups (Figure 6B). To further elucidate the anti-pigmenting function of TRF, we assessed the tyrosinase activities of the BL-induced cells. There was a drastic increase in tyrosinase activity after BL exposure. While both α TP and TRF were able to decrease the activity level, TRF appeared to exhibit a more pronounced effect (Figure 6C).

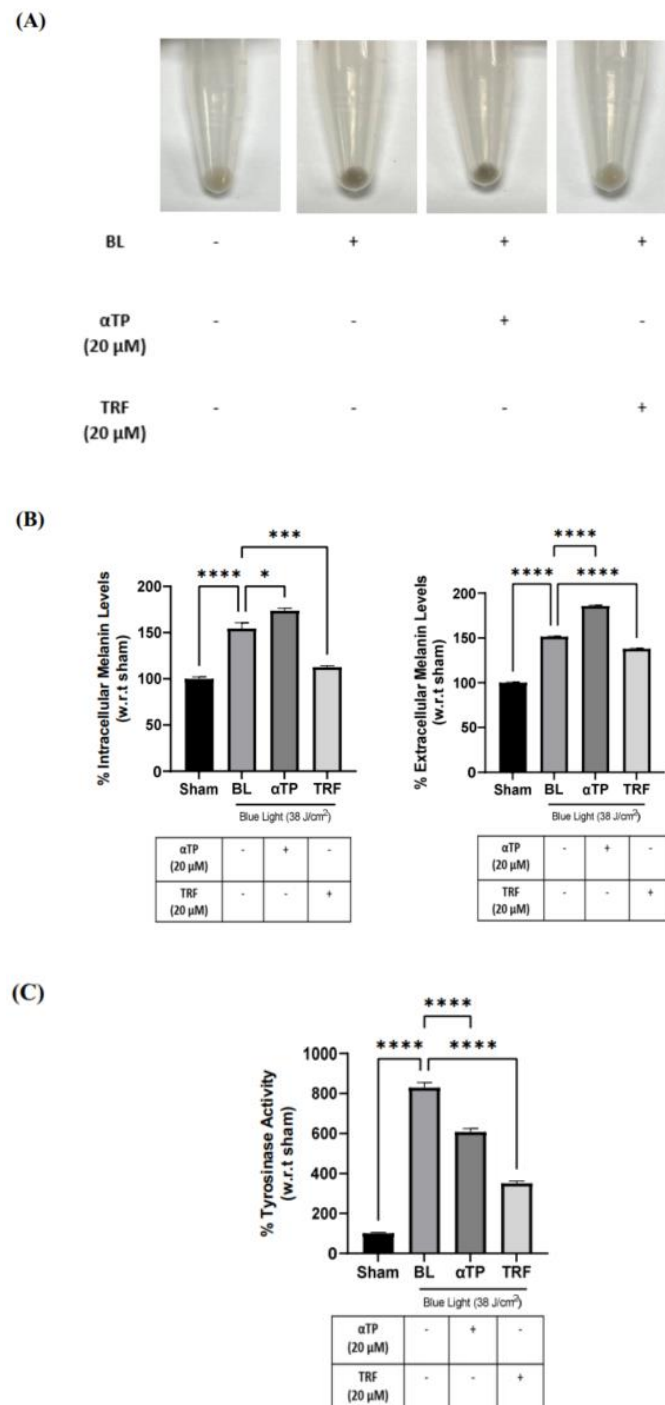


Figure 6. Pigmentation effects of BL on B16-F1 melanocytes and protective effects of TRF on melanogenesis process. (A) B16-F1 cell pellet colour after BL exposure and treatments. (B) Intracellular and extracellular melanin levels of cells induced by BL and treatment. (C) Tyrosinase activity in B16-F1 cells after BL and treatment. Data shown are expressed as % of sham and expressed as mean \pm SEM. **** $p < 0.0001$, *** $p < 0.001$, and * $p < 0.05$ represent statistical significance.

2.7. TRF Exhibited Anti-Melanogenic Effects

Based on the results obtained in Section 2.6, which exhibit the promising effects of TRF in preventing BL-induced hyperpigmentation, we aimed to further investigate the effects of TRF on pigmentation. To understand the mode of action behind the anti-pigmenting properties of TRF, we conducted the same melanin and tyrosinase assay on the B16-F1 cells. The B16-F1 cells were treated with α TP and TRF in the absence of BL induction. Similar to

previous experiments, changes in cell pellet colour, melanin levels, and tyrosinase activity were measured. The TRF-treated cells exhibited a lighter pellet colour compared to the non-treated and α TP-treated cells (Figure 7A). This finding is supported by the quantification levels regarding intra- and extracellular melanin levels, along with the measurement of tyrosinase activity in the cells. Remarkably, TRF treatment resulted in a significant reduction in melanin levels and tyrosinase activity (Figure 7B). These findings demonstrate that TRF may exhibit anti-melanogenic properties by modulating tyrosinase activity in the cells.

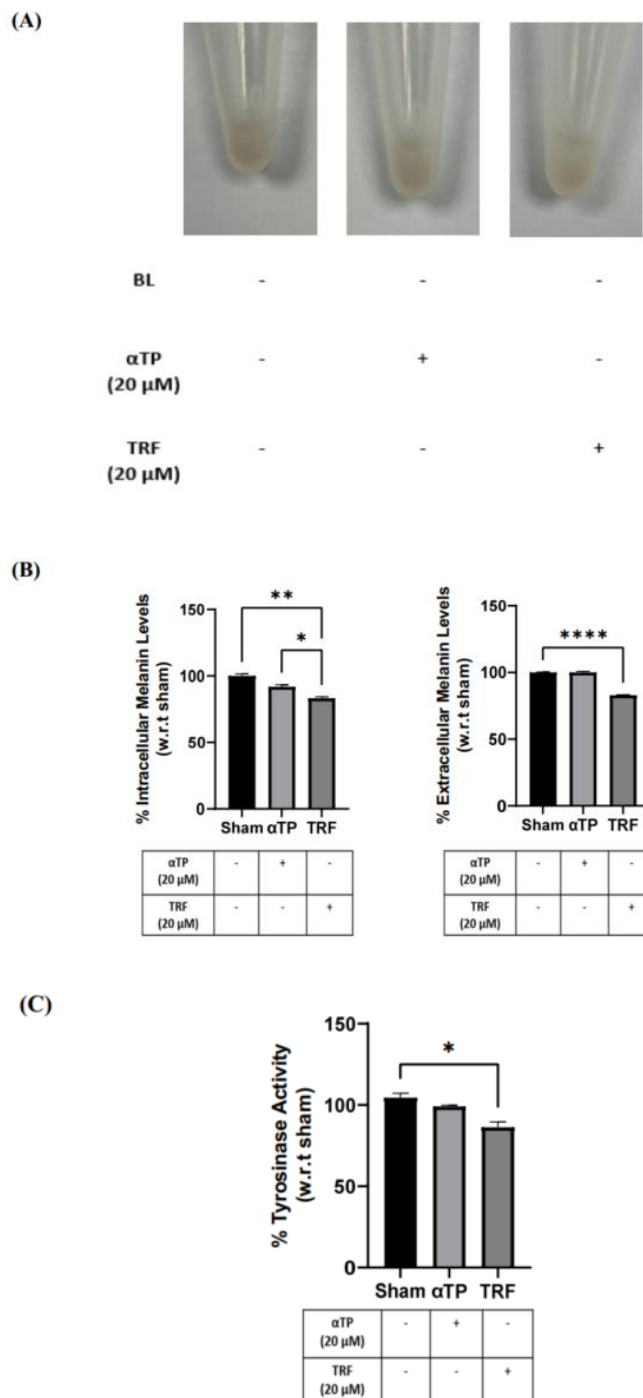


Figure 7. Pigmentation effects of α TP and TRF on the melanogenesis process. (A) B16-F1 cell pellet colour after treatments. (B) Intracellular and extracellular melanin levels of cells. (C) Tyrosinase activity in B16-F1 cells. Data shown are expressed as % of sham and expressed as mean \pm SEM. **** $p < 0.0001$, ** $p < 0.01$, and * $p < 0.05$ represent statistical significance.

3. Discussion

In our modern, fast-paced, and digitalized world, we are constantly surrounded by devices that emit BL, leading to an increase in the production of ROS. Melanin, a photoprotective and redox-active pigment, is produced in response to the increased oxidative stress caused by exposure to ROS. This pro-oxidative state triggers an upregulation of melanin production, resulting in skin darkening and hyperpigmentation [21]. Our study involved investigating the anti-oxidative, anti-apoptotic, and anti-melanogenic properties of TRF in BL-exposed B16-F1 melanocytes. Additionally, we also aimed to elucidate the molecular mechanisms underlying BL-induced apoptosis and pigmentation.

BL exposure is known to generate a significant amount of superoxide ROS, leading to cellular inflammation and oxidative stress. Under normal circumstances, our cells possess their own anti-oxidative systems that can eliminate the generated ROS. However, BL is known to oxidize the anti-oxidants produced by the cell, compromising the cell's anti-oxidative capacity [22]. When a cell undergoes oxidative stress, it can result in irreversible damage. If the cell's endogenous repair mechanisms are unable to rapidly address this damage, it can accumulate and ultimately lead to cell death [23]. In our study, we observed an increase in ROS levels in the B16-F1 cells exposed to BL. However, both treatments, α TP and TRF, were effective in reducing the ROS produced, with TRF exhibiting a more significant protective effect. T3s act as a potent anti-oxidant, scavenging free radicals more effectively than α TP due to their structural differences, which allow for better penetration. Furthermore, γ T3s and TRF have been reported to possess various anti-oxidative properties, such as preventing a reduction in the expression of the enzyme superoxide dismutase (SOD) [24,25]. The regulation of SOD activity is crucial, as it is the only enzyme that exclusively interacts with superoxide, helping to keep the levels of ROS at a minimum in cells [26]. Therefore, our treatment with TRF might be beneficial in suppressing the formation of BL-induced superoxide, thereby protecting the cells from a pro-oxidative state.

The accumulation of ROS in cells can activate various signalling pathways, including apoptosis or necrosis-related pathways [27]. One of the major pathways involved in cellular apoptosis is the MAPK pathway. MAPK signalling cascades play a role in numerous physiological processes, such as proliferation, differentiation, inflammation, and apoptosis. Among the different MAPK subgroups, p38 is often activated in response to oxidative stress, inflammation, and DNA damage [28,29]. The activation of the p38 molecule is denoted by phosphorylation and can lead to either an intrinsic apoptotic pathway, activated by internal cell stresses, or an extrinsic apoptotic pathway, typically activated by external stimuli [30]. Oxidative stress within cells, as part of the intrinsic pathway, can contribute to the activation of pro-apoptotic factors, resulting in mitochondrial membrane permeabilization and alterations in mitochondrial membrane potential. This triggers a cascade of signalling events, including the release of the apoptogenic factor cytochrome c from the mitochondria into the cytoplasm. Cytochrome c in the cytosol then forms a complex with apoptotic protease activating factor-1 and caspase-9, further activating caspases such as caspase-3 and ultimately leading to cellular destruction [9,31].

In this study, we investigated the effect of TRF on the activity of the p38 MAPK molecule and the mitochondria-mediated apoptotic pathway. Our results showed that TRF effectively abolished the activation of the p38 molecule, improved the mitochondrial membrane potential, and reduced the expression of cleaved caspase-3. In a previous research study, Satyamitra et al. [32] reported that γ T3, an isomer found in TRF, can suppress the activities of caspase-3 and caspase-7, but it does not affect the levels of cytochrome c. This suggests that γ T3 may not directly rescue mitochondrial function. Additionally, a previous study substantiates our findings by showing that treatment with TRF can lower levels of ROS and MAPK proteins, which are precursors of oxidative stress [16]. Based on these observations, we theorize that TRF rescues B16-F1 cells exposed to BL due to its anti-oxidative nature, thereby terminating the downstream apoptotic signalling cascade. Further studies are warranted to elucidate the role and mode of action of TRF in the mitochondria-mediated apoptotic pathway.

Our study demonstrated that prolonged BL exposure increased the rate of melanogenesis in B16-F1 cells by modulating tyrosinase activity. Tyrosinase and dopachrome tautomerase are the key limiting enzymes involved in melanogenesis, which is the process of skin pigmentation [33]. During melanogenesis, the formation of dopaquinone (DQ) is a rate-limiting step and is produced when L-tyrosine is oxidized by tyrosinase. The produced DQ then undergoes subsequent reactions to produce either pheomelanin or eumelanin, making tyrosinase a key enzyme in melanogenesis [34]. In addition to tyrosinase, melanin synthesis in melanocytes is regulated by microphthalmia-associated transcription factor (MITF), which is the master gene of melanocyte development and can be activated by various external stimuli, including the MAPK signalling pathway [35].

In our study, TRF exhibited anti-melanogenic properties by reducing the levels of intra- and extracellular melanin produced upon BL induction. This could be attributed to the anti-oxidative functions of TRF. Furthermore, our results also established that TRF inhibited melanogenesis by modulating tyrosinase activity, suggesting that TRF may have a direct effect on melanin synthesis. Although the expression of MITF would be crucial in discussing the melanogenic pathways, our findings showed a significant decrease in tyrosinase activity with TRF treatment. Considering that tyrosinase expression is tightly regulated by MITF, it is plausible to consider that TRF may also exert an inhibitory effect on MITF expression [36].

Our experimental design provided quantitative evidence that supports our hypothesis and enhances our understanding of the effects of BL on melanocytes. To the best of our knowledge, this is the first study to demonstrate the efficacy and protective effects of TRF against BL-induced oxidative stress and melanogenesis, particularly in comparison with α TP, which is a more commonly used active ingredient in the skin care market. However, we acknowledge that there are certain limitations to this study. To gain a more comprehensive understanding of the mode of action of TRF, further molecular research is needed. Specifically, the use of inhibitors targeting various signalling pathways, such as p38-MAPK, which regulates mitochondrial apoptosis and melanogenesis, would be beneficial in elucidating the precise mechanism by which TRF exerts its effects. This would provide deeper insights into the molecular pathways involved in the protective actions of TRF against BL-induced oxidative stress and melanogenesis. Moreover, to validate the protective effects of TRF on BL-induced skin damage, additional randomized controlled clinical trials are also needed.

4. Materials and Methods

For our study, we conducted various assays to investigate the protective effects of TRF on BL-exposed melanocytes. Sections 4.1 and 4.2 list the cell culture reagents used and treatment preparation. Section 4.3 outlines the BL panel parameters. Sections 4.4 and 4.5 describe the MTT proliferative assay and the apoptosis assay, the latter of which was carried out via flow cytometry. Sections 4.6 and 4.7 describe the fluorescence imaging analysis for ROS and mitochondrial membrane potential. Sections 4.8 and 4.9 detail the melanogenesis rate and tyrosinase activity measurements. Section 4.10 explains the Western blotting protocol, and Section 4.11 states the statistical analysis protocols utilized for this study.

4.1. Cell Culture and Reagents

Murine melanoma B16-F1 cell line (CRL-6323) was purchased from American Type Culture Collection (ATCC, Manassas, VA, USA). The cells were cultured in Dulbecco's modified Eagle's Medium (DMEM; Nacalai Tesque Inc., Kyoto, Japan) supplemented with 10% (*v/v*) foetal bovine serum (HyClone Laboratories, Logan, UT, USA) and 1% (*v/v*) penicillin G (100 U/mL) and streptomycin (100 μ g/mL) (gibco, Thermo Scientific, Waltham, MA, USA). The cells were grown and maintained at 37 °C with 5% CO₂ and humidity. Monoclonal antibodies against phospho-p38, total p38, and cleaved caspase 3 were obtained from Cell Signaling Technology (Danvers, MA, USA). A monoclonal antibody against β -actin was obtained from Santa Cruz Biotechnology (Santa Cruz, CA, USA).

Phosphate buffered saline (PBS), 0.05% trypsin, and phenol red-free DMEM were purchased from Gibco (Thermo Scientific). Dimethyl sulfoxide (DMSO) was purchased from Kanto Chemical Co. (Tokyo, Japan). Methanol and absolute ethanol were purchased from Fisher Scientific (Thermo Scientific). MTT, α TP, synthetic melanin, L-3,4-dihydroxyphenylalanine (L-DOPA), bovine serum albumin (BSA), DCFDA, and JC-1 kit were obtained from Sigma-Aldrich (St. Louis, MO, USA). TRF with a purity of $\geq 95\%$ was supplied by Davos Life Science Sdn Bhd (DavosLife E3, Petaling Jaya, Malaysia).

4.2. Natural Extract and Cell Treatment

The TRF and α TP stock solution were prepared in absolute ethanol at a concentration of 100 mM and stored at $-20\text{ }^{\circ}\text{C}$. The stocks were then diluted in complete DMEM or phenol red-free DMEM to a final concentration of 20 μM for each treatment. The B16-F1 cells were incubated with the respective treatments for 24 h before irradiation, during the irradiation, and after irradiation where necessary.

4.3. Cell Irradiation

The B16-F1 cells were subjected to artificial BL irradiation with the aim of inducing oxidative stress and melanin synthesis within the melanocytes. The BL source was a panel of LED light bulbs (15×15) with a power of $3.6\text{ mW}/\text{cm}^2$, which emitted light at 465 nm (HQRP, Harrison, NJ, USA) and were placed in a customized WCI-40 CO_2 incubator (Bio Laboratories Pte Ltd., Singapore). The B16-F1 cells were exposed to a BL irradiation dosage of $38\text{ J}/\text{cm}^2$, which is equivalent to 3 h of in vitro BL exposure. Immediately after irradiation, fresh media with the respective treatments were added, and the cells were maintained in the CO_2 incubator.

4.4. MTT Cell Viability Assay

The B16-F1 cells were cultured in the individual wells of a 96-well plate at a density of 5×10^3 cells/well for 24 h. The cell viability of the cells was measured 24 h after BL irradiation. MTT solution (0.5 mg/mL) was added into each well for 2 h and incubated at $37\text{ }^{\circ}\text{C}$ with 5% CO_2 and humidity. The formazan crystals were dissolved in 200 μL of DMSO, and the absorbance was measured at 595 nm using the Enspire[®] Multimode Plate Reader (Perkin Elmer, Waltham, MA, USA).

4.5. Annexin-V Assay by Flow Cytometry

Cellular death was assessed by using the Dead Cell Apoptosis Kit with Annexin V (Thermo Scientific) according to the manufacturer's protocol. The cells were cultured in 60 mm Petri dishes at a density of 2×10^5 cells/dish for 24 h. At 24 h after BL exposure, the cells were harvested by trypsinization, washed twice in ice cold PBS, and resuspended in $1 \times$ annexin-binding buffer at a concentration of 1×10^6 cells/mL. The samples were then used for flow cytometry analysis using the Accuri[™] C6 Plus System (Becton Dickson, Franklin Lakes, NJ, USA).

4.6. Intracellular ROS Assay

The B16-F1 cells were cultured in 6-well plates at a density of 0.8×10^6 cells/well for 24 h. Immediately after BL irradiation, the cell culture medium was aspirated, and the cells were incubated with 10 μM of DCFDA dye for 30 min in the dark at $37\text{ }^{\circ}\text{C}$. The cells were then washed twice in PBS, and microscopic images were obtained using the EVOS M5000 Imaging System (Thermo Scientific) with a green excitation filter. Fluorescence intensity was then analysed using ImageJ version 1.8.0_172 (National Institutes of Health, Bethesda, MD, USA), and data were normalized with respect to the respective sham values.

4.7. Mitochondrial Membrane Potential

To assess mitochondrial membrane potential, the JC-1 assay was conducted. The B16-F1 cells were cultured in 60 mm Petri dishes at a density of 2×10^5 cells/dish for

24 h. Immediately after BL irradiation, the cell culture medium was aspirated, and the cells were incubated with 5 µg/mL of JC-1 dye for 20 min in the dark at 37 °C. Subsequently, the cells were washed twice in incomplete DMEM. Microscopic images were obtained using an inverted microscope (Eclipse TE2000-U, Nikon, Minato City, Tokyo, Japan) with orange–red and green filters emitted from a Nikon Intensilight C-HGFI. Images were captured using a Nikon Digital Sight DS-U2. Fluorescence intensity was analysed using ImageJ version 1.8.0_172 (National Institutes of Health), and data were normalized with respect to the respective sham values.

4.8. Intracellular and Extracellular Melanin Content

The B16-F1 cells were cultured in 60 mm Petri dishes at a density of 2×10^5 cells/dish for 24 h. After 24 h, the cells were harvested by scraping, and the cell culture medium were collected. The cells were then incubated at 60 °C at 1 h in 1 M NaOH and vortexed to solubilize the melanin pigments. Following that, the cell suspensions and culture medium were centrifuged at $1500 \times g$ rpm for 15 min. The absorbance was then measured at 405 nm using the EnSpire[®] Multimode Plate Reader (Perkin Elmer) and compared to a standard curve prepared using synthetic melanin. Thereafter, the intracellular and extracellular melanin contents were determined based on absorbance/µg of protein. The protein content was determined using the DC protein assay kit (Bio-Rad, Hercules, CA, USA).

4.9. Tyrosinase Activity

Cellular tyrosinase activity was determined as reported by Lee et al. with slight modifications [37]. The cells were cultured in 60 mm Petri dishes at a density of 2×10^5 cells/dish for 24 h. At 24 h after irradiation and treatment, the cells were washed with PBS and collected with lysis buffer. The cells were then ruptured by freezing for 30 min in -80 °C, followed by thawing on ice. Afterwards, the lysate was clarified by centrifugation at $13,000 \times g$ rpm for 20 min at 4 °C. The protein content was determined using the DC protein assay (Bio-Rad). An equal amount of protein was then added into each well of a 96-well plate, followed by 10% of 2 mg/mL L-DOPA prepared in phosphate solution. The well plate was then incubated at 37 °C for 1 h, and the absorbance of the mixture was measured using the EnSpire[®] Multimode Plate Reader (Perkin Elmer).

4.10. Western Blot

Whole lysates were collected by resuspending the cell pellets with RadioImmunoPrecipitation Assay (RIPA) lysis buffer containing 50 mM Tris-HCl pH 8.0, 150 mM sodium chloride, 1 mM ethylenediaminetetraacetic acid, 1% *v/v* nonidet P-40, 0.5% *v/v* sodium deoxycholate, and 0.1% *v/v* sodium dodecyl sulfate supplemented with protease and phosphatase cocktail inhibitors (Roche, Basel, Switzerland). The protein concentration was determined using the DC Protein Assay Kit (Bio-Rad) according to the manufacturer's instructions, and protein standards were prepared using BSA. The protein samples were then prepared and loaded onto polyacrylamide gel electrophoresis at 20 mA for 1 h using the Mini-PROTEAN 3 Cell (Bio-Rad). The membrane was then blocked with 10% *v/v* non-fat milk in Tris-buffered Saline (TBS) supplemented with 0.1% *v/v* Tween-20 (TBS-T). Subsequently, the blots were washed twice with TBS-T and then incubated with the corresponding antibodies at 4 °C overnight. The blots were then washed thrice with TBS-T to remove the unbound primary antibodies before exposure to IgG-HRP-conjugated secondary antibodies in 5% *v/v* non-fat milk in TBS-T for 1 h at room temperature (25 °C). The unbound secondary antibodies were removed by being washed thrice with TBS-T. Chemiluminescent protein bands were then visualized by ECL Select Western Blot Detection Reagent (Amersham, Piscataway, NJ, USA) using the ChemiDoc MP Imaging System, and ImageLab TM software version 6.1 (both from Bio-Rad) was used for densitometric analysis.

4.11. Statistical Analysis

All results are expressed as the mean \pm standard error of the mean (SEM), and the data obtained were statistically evaluated via a one-way analysis of variance (ANOVA), followed by Tukey's multiple comparisons test carried out using GraphPad Prism 9.4.1 (GraphPad Software, San Diego, CA, USA). A p value of <0.05 (*) was considered to be statistically significant.

5. Conclusions

Exposing the skin to BL for a prolonged period of time can disrupt skin health by generating ROS and causing hyperpigmentation, which can accelerate skin ageing [38]. BL also has detrimental effects on mitochondrial health, leading to a decline in cell function and, eventually, cell death [39]. Our study demonstrated that BL exposure induced cell death and hyperpigmentation in melanocytes. However, treatment with TRF was able to protect melanocytes from cell death and hyperpigmentation, potentially through the regulation of ROS and mitigation of mitochondria damage. TRF treatment also provided anti-pigmentation properties by regulating tyrosinase activity. In summary, our results indicate that TRF exhibits more robust protective effects against BL-induced damage in melanocytes compared to α TP through a combination of anti-oxidative and anti-melanogenic mechanisms (Figure 8). These findings support the potential of TRF as an active agent for protecting melanocytes from BL-induced damage. Future research, including human clinical trials, are needed to validate the effects of TRF on human skin.

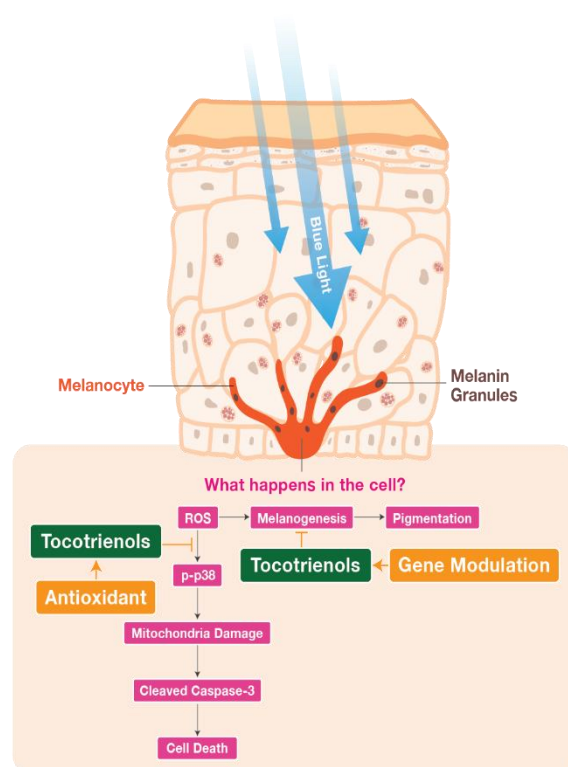


Figure 8. Schematic diagram illustrates the suggested mechanisms underlying the anti-oxidative and anti-melanogenic effects of TRF in BL-induced cellular stress and melanogenesis in B16-F1 cells. TRF effectively reduces the ROS production induced by BL, thereby inhibiting the activation of the p38 MAPK molecule. This inhibition subsequently protects the mitochondrial membrane potential of the cells and prevents cell death. Additionally, TRF demonstrates the ability to ameliorate the hyperpigmentation effects induced by BL through its ROS-protecting properties and modulation of tyrosinase activity in B16-F1 cells.

Author Contributions: Conceptualization, W.N.Y. and Y.W.U.; Methodology, J.R.E.N. and W.N.Y.; Validation, J.R.E.N. and W.N.Y.; Formal analysis, J.R.E.N.; Investigation, J.R.E.N. and W.N.Y.; Data curation, J.R.E.N.; Writing—original draft preparation, J.R.E.N.; Writing—review and editing, J.R.E.N., W.N.Y. and Y.W.U.; Supervision, W.N.Y.; Project administration, J.R.E.N. and C.W.L.T.; Funding acquisition, W.N.Y. and Y.W.U. All authors have read and agreed to the published version of the manuscript.

Funding: This work was supported financially by a research fund from KL-Kepong Oleomas (KLK Oleo) to Davos Life Science Pte Ltd., under fund number DLS-2021—Skin.

Institutional Review Board Statement: Not applicable.

Informed Consent Statement: Not applicable.

Data Availability Statement: No new data were created or analysed in this study. Data sharing is not applicable to this article.

Acknowledgments: The authors wish to extend their special thanks to Vincent Boey Ying Shiun for the Figure 8.

Conflicts of Interest: Juvenia Rui En Neo and Wei Ney Yap work for Davos Life Science (a subsidiary of KLK Oleo). Cheryl Wei Ling Teo is an ex-employee of Davos Life Science. Yee Wei Ung works for KLK Oleo, a manufacturer of tocotrienols.

References

1. Krutmann, J.; Bouloc, A.; Sore, G.; Bernard, B.A.; Passeron, T. The skin aging exposome. *J. Dermatol. Sci.* **2017**, *85*, 152–161. [[CrossRef](#)] [[PubMed](#)]
2. Chambers, E.S.; Vukmanovic-Stejic, M. Skin barrier immunity and ageing. *Immunology* **2020**, *160*, 116–125. [[CrossRef](#)] [[PubMed](#)]
3. Passeron, T.; Coelho, S.G.; Miyamura, Y.; Takahashi, K.; Hearing, V.J. Immunohistochemistry and in situ hybridization in the study of human skin melanocytes. *Exp. Dermatol.* **2007**, *16*, 162–170. [[CrossRef](#)]
4. de Assis, L.V.M.; Tonolli, P.N.; Moraes, M.N.; Baptista, M.S.; de Lauro Castrucci, A.M. How does the skin sense sun light? An integrative view of light sensing molecules. *J. Photochem. Photobiol. C Photochem. Rev.* **2021**, *47*, 100403. [[CrossRef](#)]
5. Modenese, A.; Korpinen, L.; Gobba, F. Solar radiation exposure and outdoor work: An underestimated occupational risk. *Int. J. Environ. Res. Public Health* **2018**, *15*, 2063. [[CrossRef](#)]
6. O'Hagan, J.B.; Khazova, M.; Price, L.L. Low-energy light bulbs, computers, tablets and the blue light hazard. *Eye* **2016**, *30*, 230–233. [[CrossRef](#)]
7. Lorrio, S.; Rodriguez-Luna, A.; Delgado-Wicke, P.; Mascaraque, M.; Gallego, M.; Perez-Davo, A.; González, S.; Juarranz, Á. Protective effect of the aqueous extract of *deschampsia antarctica* (EDAFENCE((R))) on skin cells against blue light emitted from digital devices. *Int. J. Mol. Sci.* **2020**, *21*, 988. [[CrossRef](#)]
8. Portillo, M.; Mataix, M.; Alonso-Juarranz, M.; Lorrio, S.; Villalba, M.; Rodriguez-Luna, A.; González, S. The aqueous extract of *polypodium leucotomos* (Fernblock((R))) regulates opsin 3 and prevents photooxidation of melanin precursors on skin cells exposed to blue light emitted from digital devices. *Antioxidants* **2021**, *10*, 400. [[CrossRef](#)]
9. Oh, P.S.; Na, K.S.; Hwang, H.; Jeong, H.S.; Lim, S.; Sohn, M.H.; Jeong, H.J. Effect of blue light emitting diodes on melanoma cells: Involvement of apoptotic signaling. *J. Photochem. Photobiol. B* **2015**, *142*, 197–203. [[CrossRef](#)]
10. Sato, K.; Minai, Y.; Watanabe, H. Effect of monochromatic visible light on intracellular superoxide anion production and mitochondrial membrane potential of B16F1 and B16F10 murine melanoma cells. *Cell Biol. Int.* **2013**, *37*, 633–637. [[CrossRef](#)]
11. Baek, J.; Lee, M.G. Oxidative stress and antioxidant strategies in dermatology. *Redox Rep.* **2016**, *21*, 164–169. [[CrossRef](#)] [[PubMed](#)]
12. Mohd Zaffarin, A.S.; Ng, S.F.; Ng, M.H.; Hassan, H.; Alias, E. Pharmacology and pharmacokinetics of vitamin E: Nanoformulations to enhance bioavailability. *Int. J. Nanomed.* **2020**, *15*, 9961–9974. [[CrossRef](#)] [[PubMed](#)]
13. Berardesca, E.; Cameli, N. Vitamin E supplementation in inflammatory skin diseases. *Dermatol. Ther.* **2021**, *34*, e15160. [[CrossRef](#)] [[PubMed](#)]
14. Thiele, J.J.; Ekanayake-Mudiyanselage, S. Vitamin E in human skin: Organ-specific physiology and considerations for its use in dermatology. *Mol. Asp. Med.* **2007**, *28*, 646–667. [[CrossRef](#)]
15. Kanchi, M.M.; Shanmugam, M.K.; Rane, G.; Sethi, G.; Kumar, A.P. Tocotrienols: The unsaturated sidekick shifting new paradigms in vitamin E therapeutics. *Drug Discov. Today* **2017**, *22*, 1765–1781. [[CrossRef](#)]
16. Neo, J.R.E.; Teo, Z.N.; Yeo, J.S.E.; Ng, C.K.S.; Teo, C.W.L.; Ung, Y.W.; Yap, W.N. Tocotrienols improve urban particulate matter-induced skin damages by regulating skin barrier function and ROS/MAPK signalling pathway in keratinocytes. *Atmos. Pollut. Res.* **2022**, *13*, 101564. [[CrossRef](#)]
17. Yap, W.N.; Zaiden, N.; Xu, C.H.; Chen, A.; Ong, S.; Teo, V.; Yap, Y.L. Gamma- and delta-tocotrienols inhibit skin melanin synthesis by suppressing constitutive and UV-induced tyrosinase activation. *Pigment Cell Melanoma Res.* **2010**, *23*, 688–692. [[CrossRef](#)]
18. Rascalou, A.; Lamartine, J.; Poydenot, P.; Demarne, F.; Bechetoille, N. Mitochondrial damage and cytoskeleton reorganization in human dermal fibroblasts exposed to artificial visible light similar to screen-emitted light. *J. Dermatol. Sci.* **2018**, *91*, 195–205. [[CrossRef](#)]

19. Sivandzade, F.; Bhalerao, A.; Cucullo, L. Analysis of the Mitochondrial Membrane Potential Using the Cationic JC-1 Dye as a Sensitive Fluorescent Probe. *Bio Protoc.* **2019**, *9*, e3128. [[CrossRef](#)]
20. Cui, S.; Nian, Q.; Chen, G.; Wang, X.; Zhang, J.; Qiu, J.; Zhang, Z. Ghrelin ameliorates A549 cell apoptosis caused by paraquat via p38-MAPK regulated mitochondrial apoptotic pathway. *Toxicology* **2019**, *426*, 152267. [[CrossRef](#)]
21. Solano, F. Photoprotection and skin pigmentation: Melanin-related molecules and some other new agents obtained from natural sources. *Molecules* **2020**, *25*, 1537. [[CrossRef](#)] [[PubMed](#)]
22. Nakashima, Y.; Ohta, S.; Wolf, A.M. Blue light-induced oxidative stress in live skin. *Free Radic. Biol. Med.* **2017**, *108*, 300–310. [[CrossRef](#)] [[PubMed](#)]
23. Navarro-Yepes, J.; Burns, M.; Anandhan, A.; Khalimonchuk, O.; del Razo, L.M.; Quintanilla-Vega, B.; Pappa, A.; Panayiotidis, M.I.; Franco, R. Oxidative stress, redox signaling, and autophagy: Cell death versus survival. *Antioxid. Redox Signal.* **2014**, *21*, 66–85. [[CrossRef](#)]
24. Jiang, Q. Natural forms of vitamin E: Metabolism, antioxidant, and anti-inflammatory activities and their role in disease prevention and therapy. *Free Radic. Biol. Med.* **2014**, *72*, 76–90. [[CrossRef](#)] [[PubMed](#)]
25. Ranasinghe, R.; Mathai, M.; Zulli, A. Revisiting the therapeutic potential of tocotrienol. *Biofactors* **2022**, *48*, 813–856. [[CrossRef](#)] [[PubMed](#)]
26. Wang, Y.; Branicky, R.; Noe, A.; Hekimi, S. Superoxide dismutases: Dual roles in controlling ROS damage and regulating ROS signaling. *J. Cell Biol.* **2018**, *217*, 1915–1928. [[CrossRef](#)]
27. Redza-Dutordoir, M.; Averill-Bates, D.A. Activation of apoptosis signalling pathways by reactive oxygen species. *Biochim. Biophys. Acta* **2016**, *1863*, 2977–2992. [[CrossRef](#)] [[PubMed](#)]
28. Johnson, G.L.; Lapadat, R. Mitogen-activated protein kinase pathways mediated by ERK, JNK, and p38 protein kinases. *Science* **2002**, *298*, 1911–1912. [[CrossRef](#)] [[PubMed](#)]
29. Zhang, W.; Liu, H.T. MAPK signal pathways in the regulation of cell proliferation in mammalian cells. *Cell Res.* **2002**, *12*, 9–18. [[CrossRef](#)]
30. Grab, J.; Rybniker, J. The expanding role of p38 mitogen-activated protein kinase in programmed host cell death. *Microbiol. Insights* **2019**, *12*, 1178636119864594. [[CrossRef](#)]
31. Eskandari, E.; Eaves, C.J. Paradoxical roles of caspase-3 in regulating cell survival, proliferation, and tumorigenesis. *J. Cell Biol.* **2022**, *221*, e202201159. [[CrossRef](#)] [[PubMed](#)]
32. Satyamitra, M.; Ney, P.; Graves, J., 3rd; Mullaney, C.; Srinivasan, V. Mechanism of radioprotection by delta-tocotrienol: Pharmacokinetics, pharmacodynamics and modulation of signalling pathways. *Br. J. Radiol.* **2012**, *85*, e1093–e1103. [[CrossRef](#)] [[PubMed](#)]
33. Lee, A.Y. Skin pigmentation abnormalities and their possible relationship with skin aging. *Int. J. Mol. Sci.* **2021**, *22*, 3727. [[CrossRef](#)] [[PubMed](#)]
34. Pillaiyar, T.; Manickam, M.; Namasivayam, V. Skin whitening agents: Medicinal chemistry perspective of tyrosinase inhibitors. *J. Enzyme Inhib. Med. Chem.* **2017**, *32*, 403–425. [[CrossRef](#)]
35. Shim, S.Y.; Lee, Y.E.; Lee, M. Antioxidant compounds, kirenol and methyl ent-16alpha, 17-dihydroxy-kauran-19-oate bioactivity-guided isolated from siegesbeckia glabrescens attenuates MITF-mediated melanogenesis via inhibition of intracellular ROS production. *Molecules* **2021**, *26*, 1940. [[CrossRef](#)]
36. Yu, F.; Lu, Y.; Zhong, Z.; Qu, B.; Wang, M.; Yu, X.; Chen, J. Mitf involved in innate immunity by activating tyrosinase-mediated melanin synthesis in pteris penguin. *Front. Immunol.* **2021**, *12*, 626493. [[CrossRef](#)]
37. Lee, Y.S.; Kim, D.W.; Kim, S.; Choi, H.I.; Lee, Y.; Kim, C.D.; Lee, J.H.; Do Lee, S.; Lee, Y.H. Downregulation of NFAT2 promotes melanogenesis in B16 melanoma cells. *Anat. Cell Biol.* **2010**, *43*, 303–309. [[CrossRef](#)]
38. Suitthimeathegorn, O.; Yang, C.; Ma, Y.; Liu, W. Direct and indirect effects of blue light exposure on skin: A review of published literature. *Skin Pharmacol. Physiol.* **2022**, *35*, 305–318. [[CrossRef](#)]
39. Godley, B.F.; Shamsi, F.A.; Liang, F.Q.; Jarrett, S.G.; Davies, S.; Boulton, M. Blue light induces mitochondrial DNA damage and free radical production in epithelial cells. *J. Biol. Chem.* **2005**, *280*, 21061–21066. [[CrossRef](#)]

Disclaimer/Publisher's Note: The statements, opinions and data contained in all publications are solely those of the individual author(s) and contributor(s) and not of MDPI and/or the editor(s). MDPI and/or the editor(s) disclaim responsibility for any injury to people or property resulting from any ideas, methods, instructions or products referred to in the content.